Shanmugasundaram *et al.*
Micro and Nano Systems Letters (2024) 12:3
https://doi.org/10.1186/s40486-023-00196-5

Micro and Nano Systems Letters

REVIEW

Open Access

SnO_2 nanostructure-based acetone sensors for breath analysis

Arunkumar Shanmugasundaram[1,2], Karthikeyan Munirathinam[1] and Dong-Weon Lee[1,2,3*]

Abstract

The World Health Organization reports that metabolic disorders are responsible for a significant proportion of global mortality. Considering this, breath sensors have gained prominence as effective tools for monitoring and diagnosing metabolic disorders, thanks to recent advancements in science and technology. In human exhaled breath, over 870 distinct volatile organic components (VOCs) have been identified. Among several VOCs, the detection of acetone in exhaled breath has received considerable attention in biomedical applications. Research indicates a strong correlation between high acetone levels in human breath and several diseases, such as asthma, halitosis, lung cancer, and diabetes mellitus. For instance, acetone is particularly noteworthy as a biomarker in diabetes, where its concentration in exhaled breath often surpasses 1.76 parts per million (ppm), compared to less than 0.8 ppm in healthy individuals. Early diagnosis and intervention in diseases associated with elevated acetone levels, aided by such non-invasive techniques, have the potential to markedly reduce both mortality and the financial burden of healthcare. Over time, various nanostructured gas sensing technologies have been developed for detecting acetone in both ambient air and exhaled breath. This article presents a mini review of cutting-edge research on acetone gas sensing, focusing specifically on nanostructured metal oxides. It discusses critical factors influencing the performance of acetone gas sensors, including acetone concentration levels and operational temperature, which affect their sensitivity, selectivity, and response times. The aim of this review is to encourage further advancements in the development of high-performance acetone gas sensors utilizing nanostructured materials, contributing to more effective management of metabolic disorders.

Keywords Nanostructures, Metal oxides, Acetone sensors, Breath sensing, Medical diagnosis

Introduction

Human exhaled breath consists of over 870 distinct volatile organic compounds (VOCs), of which many have been identified [1, 2]. Specific categories of VOCs, including alcohols, aldehydes, acids, and ketones, are products of varied biochemical and physiological processes [2]. Certain VOCs are recognized as biomarkers for specific diseases. When the concentrations of VOCs in breath specimens surpass certain thresholds, timely diagnosis and subsequent therapeutic intervention become imperative [3]. For the detection and monitoring of various VOCs in exhaled breath, several techniques have been widely used [4–11]. Although these techniques offer excellent sensitivity, selectivity, high resolution, and quantification of VOCs, they suffer from several shortcomings, including high cost, low portability, and high resource consumption. On the other hand, nanostructure-based gas sensors have received considerable attention in environmental remediation and biomedical applications [12–15]. Unlike other techniques, breath

*Correspondence:
Dong-Weon Lee
mems@jnu.ac.kr
[1] MEMS and Nanotechnology Laboratory, School of Mechanical Engineering, Chonnam National University (CNU), Gwangju 61186, Republic of Korea
[2] Advanced Medical Device Research Center for Cardiovascular Disease, Chonnam National University (CNU), Gwangju 61186, Republic of Korea
[3] Center for Next-Generation Sensor Research and development, Chonnam National University (CNU), Gwangju 61186, Republic of Korea

Springer Open

© The Author(s) 2024. **Open Access** This article is licensed under a Creative Commons Attribution 4.0 International License, which permits use, sharing, adaptation, distribution and reproduction in any medium or format, as long as you give appropriate credit to the original author(s) and the source, provide a link to the Creative Commons licence, and indicate if changes were made. The images or other third party material in this article are included in the article's Creative Commons licence, unless indicated otherwise in a credit line to the material. If material is not included in the article's Creative Commons licence and your intended use is not permitted by statutory regulation or exceeds the permitted use, you will need to obtain permission directly from the copyright holder. To view a copy of this licence, visit http://creativecommons.org/licenses/by/4.0/.

sensors simply require the patient to breathe out into the device, providing a less invasive and more comfortable experience. Breath analysis involves measuring the concentrations of various gases in a person's breath, which can provide information about the body's metabolic processes [16–20].

Among several VOCs, the detection of acetone ($OC(CH_3)_2$) has received considerable attention in biomedical applications. The detection of acetone in exhaled breath can be indicative of diabetic ketoacidosis (DKA), a serious complication that occurs in people with diabetes [21–23]. Acetone serves as a potential biomarker for diabetes, with concentrations in the exhaled breath of diabetic individuals typically exceeding 1.76 ppm, in contrast to concentrations usually below 0.8 ppm in healthy individuals [24–27]. Therefore, the detection of acetone at relatively low concentrations requires highly sensitive and selective gas sensors.

To date, several nanostructure-based gas sensors have been proposed to detect acetone. However, the practical utility of breath sensors is limited due to their low sensitivity and selectivity. The high-temperature operation of the reported breath sensors limits their application in mobile platforms [28–32]. To improve sensor performance and reduce operating temperatures, several techniques have been proposed. Such techniques widely use the incorporation of a charge transporting layer and electro-cocatalysts [33–52] (Table 1). Although the sensing performance, such as sensitivity and selectivity, increases with the incorporation of these materials, the high humidity in exhaled breath severely affects the sensor response. To overcome these challenges, advancements in material science, sensor array technology, and data processing techniques offer promising avenues to enhance selectivity, thereby expanding their applicability in various fields such as environmental monitoring, industrial safety, and healthcare diagnostics.

In this review, we articulate a comprehensive synthesis of recent advancements in the rational functionalization of responsive nanomaterials for the detection of acetone. Particular emphasis is placed on optimizing the surface chemistry and structural attributes of the associated nanomaterials—a perspective seldom explored in existing literature within this domain. We scrutinize the properties of various nanostructured materials, their surface modifications, and the potential technological limitations affecting sensor performance in breath analysis applications.

Chemical gas sensors

Chemical gas sensors operate on the principle of detecting specific chemical compounds in the air and converting this chemical interaction into a measurable signal. The core components of these sensors include a receptor,

Table 1 Acetone sensing characteristics of the SnO_2-based gas sensors

Materials	Temp (°C)	Conc (ppm)	Response (s)	Response/recovery time (s)	Ref
Large-lateral-area SnO_2	250	5	263	10/1315	[33]
Co_3O4/SnO_2 yolk-shell nanofibers	350	100	217	0.62/46.5	[34]
s-Nb_2O_5@SnO2	250	0.5	37	230/735	[35]
GC/SnO_2-500 tubes	217	100	22	0.8/228	[36]
SnO_2-ZnO nanoparticles	240	10	140.27	108/44	[37]
Pt-SnO_2 HBLs	350	2	93.56	9.2/312	[38]
Au-SnO2 nanosheets	240	100	18.18	5/66	[39]
$SnSe_2/SnO_2$ NPs	300	100	10.77	130/10	[40]
ZFO/SNO	210	100	120	30/197	[41]
SU-SnO_2/α-Fe_2O_3-2.5	300	100	18.7	8/2	[42]
SiO_2@SnO_2/α-Fe_2O_3	300	100	41.8	7/23	[43]
Zn_2SnO_4/SnO_2 hollow microboxes	250	100	20.16	97/315	[44]
Ni_1Sn_3	300	5	6	2/9	[45]
Ag-decorated SnO_2 hollow nanofibers	160	200	117	6/10	[46]
TiO_2-SnO_2-TiO_2 shell-core–shell	280	1	13.3	3.6/4.5	[47]
Eu_2O_3/Au/SnO_2 ternary nanofibers	200	100	65	10/8	[48]
SnO_2-Fe_2O_3 heterostructure	280	200	16.8	5/23	[49]
Eu-doped SnO_2 nanofibers	280	100	32.2	4/3	[50]
3D hierarchical SnO_2 nanoflowers	280	20	33	9/7	[51]
In/WO_3-SnO_2 nanostructures	200	1	4.4	4/2	[52]

which is the sensitive element that interacts directly with the target gas, and a transducer, which converts the chemical interaction into an electrical signal. When the target gas comes into contact with the receptor, typically a chemically active material, a reaction occurs that changes the physical or chemical properties of the receptor. This could involve processes such as adsorption, absorption, or changes in mass or heat. The transducer, often based on technologies such as piezoelectric, optical, or electrochemical systems, detects these changes and translates them into an electrical signal that can be quantified and correlated to the concentration of the gas. For instance, in a metal oxide semiconductor (MOS) gas sensor, the receptor is the metal oxide surface that adsorbs the gas molecules. The transducer is the electrical circuit that measures changes in the conductivity of the metal oxide layer as it interacts with the gas. The signal produced is then processed and presented, usually as a digital readout of the gas concentration, to a display or control system. Through this process, chemical gas sensors provide crucial real-time data in various applications, ranging from environmental monitoring to industrial safety and medical diagnostics.

Classifications of a chemical gas sensors

Chemical gas sensors can be classified into several types based on the operating principle of the transducer, which is the component that converts a chemical signal into a measurable physical signal. According to the International Union of Pure and Applied Chemistry (IUPAC), these classifications include electrochemical, optical, microwave, and mass-based sensors. Electrochemical sensors use a reaction between the target gas and an electrolyte to produce an electrical current proportional to the gas concentration. They are highly sensitive and selective and are commonly used to detect gases. Optical sensors operate by measuring changes in light absorption or emission resulting from interactions with the gas. This category includes fiber optic sensors and photonic sensors, which are versatile and can detect a wide range of gases. Microwave sensors detect changes in the microwave absorption or emission characteristics of a gas. These sensors are less common but can be used for high-sensitivity applications, such as detecting trace gases in the atmosphere. Mass-based sensors, such as quartz crystal microbalances (QCMs), detect changes in mass on a sensitive layer as gas molecules adsorb onto the surface. These sensors are known for their precision and are utilized in environments where very low concentrations of a gas must be detected with high accuracy. Each type of sensor has its own advantages and limitations, including sensitivity, selectivity, response time, and operational conditions, which dictate their suitability for specific applications in industry, research, and safety monitoring.

Evolution of chemiresistive gas sensors: from early developments to internet of things (IoT) integration

The history of chemiresistive-based gas sensors spans several decades, marked by significant advancements in materials science, electronics, and sensor technology. These sensors, which change their electrical resistance in response to the presence of certain gases, have become crucial in various applications, from environmental monitoring to industrial safety and biomedical applications.

Early developments (1950s-1970s): The concept of chemiresistive gas sensors emerged in the mid-twentieth century with the development of semiconductor materials. Researchers noticed that certain materials, especially metal oxides like tin oxide (SnO_2), tungsten oxide (WO_3), zinc oxide (ZnO) and exhibited changes in electrical resistance when exposed to gases. This led to the first generation of gas sensors, primarily used in laboratory settings.

Advancements and commercialization (1980s-1990s): During this period, there was significant progress in understanding the interaction between gas molecules and sensor surfaces. The miniaturization of electronics and advancements in microfabrication techniques enabled the production of smaller, more sensitive, and more reliable sensors. This era also saw the commercialization of chemiresistive gas sensors in various industries, such as petrochemical and automotive, for leak detection and air quality monitoring.

Incorporation of nanotechnology (2000s-present): The advent of nanotechnology marked a revolutionary change in chemiresistive sensors. Nanomaterials, with their high surface area-to-volume ratio, offered improved sensitivity and faster response times. Materials like carbon nanotubes, graphene, and metal oxide nanomaterials with exotic nanostructures became popular choices for sensor fabrication.

Integration with electronics and IoT (2010s-present): The integration of chemiresistive gas sensors with advanced electronics and the IoT has opened new possibilities. Sensors have become smarter, capable of real-time monitoring, and can be connected to networks for data analysis and remote monitoring. This integration has enhanced the application scope, including smart homes, wearable devices, and environmental monitoring.

Key characteristics of gas sensors: defining performance and suitability

The effectiveness and applicability of these sensors are defined by several basic characteristics. These characteristics determine the suitability of a gas sensor for

specific applications and environments, guiding the selection process for various industrial, environmental, and health-related applications.

Sensor response: This is the change in the sensor's output signal (such as electrical resistance in chemiresistive sensors) due to the presence of a target gas. The response is often measured as a change in voltage, current, or resistance when the sensor is exposed to a specific concentration of gas. The sensor response of the gas sensor is typically determined as the ratio of sensor resistance in the presence of gas and the sensor resistance in the presence of air or vice versa depending on the reducing or oxidizing gas.

Sensitivity: Sensitivity refers to the ability of the sensor to detect small changes in gas concentration. It is typically defined as the change in sensor response per unit concentration of the target gas. High sensitivity is crucial for detecting low concentrations of gases.

Selectivity: This characteristic refers to the sensor's ability to respond to a specific gas in the presence of other gases. A highly selective sensor will only react to its target gas, making it essential in environments with a mixture of different gases.

Response time: The response time is the time it takes for the sensor to respond to the presence of the target gas. This includes the time to reach a certain percentage (usually 90%) of the total response after the gas is introduced.

Recovery time: This is the time taken by the sensor to return to its baseline (usually 10%) state after the target gas has been removed. A shorter recovery time is generally preferred, especially for applications requiring rapid detection cycles.

Stability: Stability refers to the sensor's ability to maintain its performance over time. A stable sensor will show little drift in its baseline or sensitivity over long periods, which is crucial for reliable and consistent measurements.

Operating temperature range: Gas sensors often require a specific temperature range to operate effectively. The range can vary widely depending on the sensor type and the materials used.

Cross-sensitivity: This aspect describes the sensor's response to gases other than the target gas. A sensor with high cross-sensitivity may give false readings in the presence of non-target gases.

Limit of detection: This is the lowest concentration of a gas that can be reliably detected by the sensor.

Durability and lifetime: The sensor's ability to withstand environmental conditions like humidity, temperature fluctuations, and exposure to chemicals, along with its operational lifespan, defines its durability and lifetime.

Temperature-dependent sensing mechanisms in metal oxide-based gas sensors

The gas sensing mechanism of metal oxide-based gas sensors varies significantly with temperature. The sensing mechanism is fundamentally tied to the interaction between the target gas and the surface of the metal oxide. The efficiency and sensitivity of metal oxide-based gas sensors are highly dependent on the operating temperature. Room temperature operation offers the advantage of low power consumption but generally provides lower sensitivity and slower response times. Moderate temperatures improve sensitivity and reaction kinetics, while high temperatures offer the best sensitivity and selectivity but can pose challenges in terms of sensor stability and longevity.

Adsorption of Ambient Oxygen at lower temperatures: At room temperature, the amount of ambient oxygen adsorbed on the surface of the metal oxide is relatively low. Oxygen molecules can adsorb onto the surface as O_2^-, O^-, or O_2^- ions, depending on the energy levels available. However, the extent of this process is limited at lower temperatures.

$$O_{2(gas)} \leftrightarrow O_{2(ads)} \tag{1}$$

$$O_{2(ads)+e^-} \leftrightarrow O^-_{2(ads)} \left(T < 100^\circ C\right) \tag{2}$$

Interaction with target gases: When a target gas such as acetone interacts with the sensor's surface, it reacts with the adsorbed oxygen ions. For acetone usually react with the oxygen ions, releasing electrons back to the metal oxide and thus decreasing the resistance. For oxidizing gases (like NO_2), they can extract electrons from the metal oxide, increasing its resistance.

Limited sensitivity: The reactions at room temperature are often not as pronounced as at higher temperatures, leading to lower sensitivity. This is due to the lower energy levels which are not sufficient to facilitate significant reactions between the gas molecules and the adsorbed oxygen.

Increased Oxygen Adsorption at moderate temperatures (around 100 ℃): As the temperature rises to about 100 ℃, more oxygen is adsorbed onto the sensor surface and ionized, due to increased energy available for the reaction.

$$O_{2^-(ads)+e^-} \leftrightarrow 2O^-_{(ads)} \left(100^\circ C < T < 300^\circ C\right) \tag{3}$$

Enhanced sensing reactions: The increase in surface oxygen ions enhances the sensor's ability to react with the target gases. This leads to a more pronounced change in resistance for both reducing and oxidizing gases.

Improved Sensitivity: The moderate increase in temperature improves the sensor's sensitivity due to more active surface reactions.

Maximum oxygen adsorption and ionization at high temperatures: At high temperatures, oxygen adsorption and ionization on the metal oxide surface reach their peak. The surface has a high concentration of oxygen ions, making it highly reactive.

$$O_{2^-(ads)+e^-} \leftrightarrow O^-_{2(ads)} \left(T > 300^\circ C \right) \quad (4)$$

Strong gas-surface interactions: The high temperature provides sufficient energy for vigorous reactions between the target gas and the adsorbed oxygen ions. This results in a significant change in the sensor's resistance.

High sensitivity and selectivity: The high-temperature environment enhances both the sensitivity and selectivity of the sensor. The reactions are more specific and pronounced, allowing for better detection and differentiation of gases.

Stability Issues: However, prolonged operation at high temperatures can lead to issues like sensor degradation, drift, and a decrease in the lifespan of the sensor due to thermal stress.

Overcoming selectivity challenges in metal oxide gas sensors

The major limitation of metal oxide-based gas sensors is their selectivity. For instance, metal oxides, like tin oxide, operate by changing their electrical resistance in the presence of certain gases. However, one of their major drawbacks is the lack of specificity: they often respond to a variety of gases, making it challenging to distinguish between different analytes in a complex environment. This issue is particularly acute in scenarios where multiple gases are present, as the sensor might react similarly to various substances, leading to inaccurate readings or false alarms. The selectivity issue in metal oxide sensors can be attributed to their working principle. These sensors rely on the interaction between the target gas molecules and the sensor's surface, leading to changes in electrical properties. However, since many gases can interact with the sensor surface in a similar manner, distinguishing between them becomes a challenge. To overcome this limitation, several methods are employed. One approach is to modify the surface of the sensor with selective catalysts or additives that enhance its sensitivity to specific gases while reducing responses to others. For instance, adding a layer of noble metals like platinum or palladium can increase the sensor's selectivity towards certain hydrocarbons. Another method involves operating the sensor at different temperatures. Since the reaction rates of gases on the sensor surface vary with temperature, adjusting the operating temperature can help in differentiating between gases based on their reaction kinetics. Additionally, using an array of sensors, each tailored to be more responsive to a particular gas, and then analyzing the collective data through pattern recognition algorithms can significantly improve selectivity. This approach, known as electronic nose technology, mimics the human olfactory system and allows for the discrimination of complex gas mixtures, thereby expanding their applicability in various fields such as environmental monitoring, industrial safety, and healthcare diagnostics.

Effect of humidity on the sensor performance

Humidity significantly impacts sensor response, a phenomenon particularly observable in breath analysis sensors operating at varying temperatures. High temperature sensors typically show less susceptibility to humidity effects compared to their low temperature counterparts. This difference can be attributed to the physical and chemical properties of the sensor materials. At higher temperatures, the increased thermal energy can overcome the binding energy of water molecules, reducing the likelihood of condensation or adsorption on the sensor surface, which would otherwise interfere with its response. Conversely, low temperature sensors are more prone to humidity interference due to the greater likelihood of water molecule adsorption, which can skew the sensor's readings by introducing additional response factors unrelated to the target analytes. To mitigate the drawbacks of humidity in breath sensing analysis, especially in low temperature sensors, several strategies can be employed. One effective approach is the use of hydrophobic coatings on the sensor surface, which repel water molecules, thereby reducing the impact of humidity. Another method is incorporating a humidity compensation algorithm within the sensor's data processing system, allowing it to distinguish between changes in sensor response due to humidity and those due to the target analytes. The use of filters represents a pivotal strategy in mitigating the impact of humidity on breath sensor technology. In this context, filters are integrated into the sensor system to selectively reduce the presence of moisture, thereby enhancing the accuracy and reliability of the sensor's readings. These filters, typically made of hydrophobic materials, are designed to allow the passage of target analytes while repelling water molecules. By doing so, they effectively minimize the direct interaction between water vapor and the sensor's active surface. This design feature is important as it allows the filter to block larger water droplets (which are a common issue in breath analysis due to the natural moisture in exhaled air) while still

permitting the passage of smaller gas molecules that are of interest in the analysis.

Important characteristics of acetone sensing

Acetone, the simplest and smallest ketone, consists of a carbonyl group (C=O) flanked by two methyl groups (CH_3). Its detection in human exhaled breath is crucial as it indicates conditions like diabetic ketoacidosis (DKA), a serious diabetes complication. Monitoring acetone levels in breath provides essential non-invasive diagnostics for diabetes management. Additionally, acetone's distinct odor, high vapor pressure, and low boiling point contribute to its volatility. Short-term acetone exposure can cause eye, nose, and throat irritation, along with headaches, dizziness, and central nervous system effects. Prolonged inhalation may lead to unconsciousness or respiratory problems. Thus, detecting acetone in human breath and the environment is vital for managing diabetes and other metabolic disorders, as well as for addressing environmental air pollution.

Acetone gas sensing mechanism

The gas sensing mechanism of metal oxide-based sensors for detecting acetone involves a series of surface reactions and changes in electrical properties. Here's how it typically works for acetone detection. The acetone gas sensing mechanism on n-type metal oxide-based gas sensors involves the adsorption of oxygen and its ionization at the sensor surface, followed by a reaction with acetone that releases electrons back into the metal oxides, decreasing its resistance. This response is influenced by various factors, including temperature, surface modifications, and sensor morphology. These sensors are thus highly effective for detecting acetone, especially in applications where sensitive and rapid detection is crucial. The possible reaction between the adsorbed oxygen ions and acetone gas on the surface of nanostructured metal oxides can be described based on the following Eqs. (5–8)

$$CH_3COCH_{3(gas)} + 8O^- \rightarrow 3CO_2 + 8e^- + 3H_2O \quad (5)$$

$$CH_3COCH_{3(gas)} + O^-_{2(ads)} \rightarrow CH_3C^+O_{(gas)} + CH_3O^-_{(gas)} + e^- \quad (6)$$

$$CH_3C^+O_{(gas)} \rightarrow CH_{3(gas)} + CO_{(gas)} \quad (7)$$

$$CO_{(gas)} + O^-_{2(ads)} \rightarrow CO_{2(gas)} + e^-(\text{conduction band}) \quad (8)$$

SnO_2 nanostructures based acetone gas sensors

SnO_2-based metal oxide gas sensors are a prominent category in the field of gas sensing due to their excellent chemical and physical and optoelectronic properties, particularly for detecting VOCs like acetone. SnO_2 is an n-type semiconductor with a wide band gap, typically around 3.6 eV. This wide band gap is fundamental to its gas sensing properties, as it allows for the modulation of its electrical conductivity in the presence of gas molecules. The sensitivity of SnO_2 sensors arises from the change in conductivity when the surface interacts with gas molecules. In the presence of reducing gases like acetone, the reactions on the sensor surface lead to a decrease in resistance, indicating the presence of the gas. SnO_2 sensors are particularly responsive to acetone, making them valuable in applications like medical diagnosis (e.g., detecting ketone levels in breath), industrial monitoring, and environmental sensing. Over the years several SnO_2 based acetone sensors have been proposed. However, most of the sensors met with limited success owing to their low response and sensitivity and selectivity towards acetone. Therefore, several research efforts were devoted to further improve the acetone sensing performance through doping with other elements or creating composites with other metal oxides. These modifications were tailored the sensor's surface properties, enhancing acetone adsorption and reaction kinetics. Those surface modified SnO_2-based sensors were detecting acetone at relatively low concentrations, making them suitable for applications requiring the detection of trace amounts of gases.

To date, several exotic SnO_2 nanostructures including flower like structures [53, 54], multishelled hollow microspheres [55], nanobelt [56, 57] and aurelia like micro-nano spheres [58] and etc. have been proposed for the acetone sensing analysis. Several studies have demonstrated that the mesoporous structure provides a larger surface area, facilitating more interaction sites for gas molecules [59–62]. This increased surface area allows for more efficient absorption of gas molecules, leading to improved sensitivity in detecting gas concentrations. Besides, the hierarchical structure, with its interconnected pores, ensures better diffusion of gas molecules throughout the sensor material. This facilitates quicker and more uniform response to changes in gas concentration. The specific pore size and structure of the mesoporous material can be tuned to be more responsive to certain gas molecules, thus enhancing the selectivity of the sensor. This means the sensor can more effectively differentiate between various types of gases. The hierarchical mesoporous structure tends to be more stable, maintaining its integrity under different environmental conditions. This stability contributes

to consistent and reliable sensor performance over time. The unique structure can facilitate better electron transport within the material, improving the transduction of the chemical interaction with gas molecules into a measurable electrical signal.

For instance, Chen et al. prepared 3D porous flower-like SnO_2 nanostructures for acetone sensing analysis. The sensor showed a significant response to 500 ppm acetone, with the response increasing at higher concentrations. For instance, at a low concentration of 20 ppm, the sensor still delivered a high response of 33 at 280 ℃. The sensor exhibited rapid response and recovery times to acetone. Specifically, the response time was 9 s, and the recovery time was 7 s. The sensor demonstrated good selectivity to acetone when tested with various gases such as formaldehyde, ethanol, ammonia, DMF and methanol at 280 ℃, highlighting its potential for specific acetone detection in diverse applications [54]. In another study Wang et al. proposed enhanced gas sensing properties of hierarchical SnO_2 nanoflower. The SnO_2 nanoflowers, about 200 nm in size, were successfully synthesized using a simple, template-free hydrothermal method. The structure was found to be fully crystalline with a large specific surface area. The SnO_2 nanoflowers exhibited high response and fast response-recovery ability for detecting acetone at an operating temperature of 170 ℃. The enhancement in gas sensing properties was attributed to their 3D hierarchical nanostructure, large specific surface area, and the small size of the secondary SnO_2 nanorods. The maximum responses reached were 29.2 for 50 ppm acetone. The SnO_2 nanoflowers-based gas sensor showed high response ability to acetone and ethanol, with a maximum response value of 29.2 to acetone at 170 ℃, while the response to other tested gases did not exceed 10. The sensor's response increased quickly with the injection of tested gases and decreased rapidly, recovering to its initial value upon the release of the gases. The sensor showed a linear response to varying concentrations of acetone and ethanol, indicating sensitive and reversible responses to both gases. For 20 ppm acetone, the response and recovery times were 3 s and 30 s, respectively [53]. In another study hierarchical SnO_2 nanoflower assembled from nanorods via a one-pot template-free hydrothermal method was prepared for acetone sensing analysis. Four types of SnO_2 films were fabricated using spin coating, involving different conditions of introducing ammonium hydroxide or acetone during the hydrothermal synthesis. The fabricated sensors were tested for various gases such as acetone, ammonia, LPG, oxygen, and benzene across a temperature range of 50 ℃ to 300 ℃. The sensor recorded high sensitivity of about 77% for acetone at 230 ℃. The device showed high sensitivity and a limit of detection (LOD) of 280 ppb for acetone. These findings indicate the potential of the SnO_2-based sensors, fabricated through molecular imprinting techniques, in detecting acetone and ammonia with high sensitivity and selectivity [63]. The hollow SnO_2 fibers were prepared using poplar catkins as a bio-template for acetone sensing analysis applications. The fibers displayed a high specific surface area of 110.1 m^2/g and maintained mesoporous structures with a narrow pore size distribution around 4.9 nm. The hollow SnO_2 fibers showed excellent gas sensing performance towards acetone. The response of SnO_2 fibers was around 1016.4 to 100 ppm acetone and 7.0 to 1 ppm acetone at 100 ℃. The optimal performance of SnO_2 fibers in detecting acetone was achieved at a relatively low temperature of 100 ℃, with the time taken to detect and then reset being roughly 9.4 and 11.5 min for 10 ppm of acetone. The sensitivity levels of the SnO_2 fibers varied significantly with the concentration of acetone; they registered approximately 2684.6, 1750.1, 1016.4, 444.8, 156.2, and 80.0 in response to 500, 300, 100, 50, 20, and 10 ppm of acetone, respectively, at 100 ℃. Furthermore, when the sensor was tested with lower concentrations of acetone at 100 ℃, specifically 5, 2, and 1 ppm, it showed sensitivities of about 36.4, 14.0, and 7.0, respectively. The authors compared the performance of the synthesized hollow SnO_2 fiber gas sensor with various other semiconductor metal oxide gas sensors, highlighting its good selectivity and high sensitivity to acetone [64]. The acetone sensor, which is based on hierarchical mesoporous SnO_2 nanotube arrays, demonstrated a remarkable response ($S = 20.3$) and maintained good linearity over a range of acetone concentrations at the ppm level (5–300 ppm), along with exceptional selectivity towards 100 ppm of acetone gas. When compared to sensors made through a slurry-coating method, these SnO_2 nanotube arrays, which are assembled in situ in a controlled manner, showed a more robust structure and a simpler manufacturing process. The superior performance in detecting acetone could be attributed to its distinct hollow structure and advantageous orientation during growth [65]. Catalyst free SnO2 nanosheet based sensor has been proposed for ppb level detection of acetone. The SnO_2 nanosheets were successfully synthesized using a SnF_2 aqueous solution at 90 ℃. These nanosheets mainly exposed the (101) crystal facets. The SnO_2 nanosheets synthesized for 6 h demonstrated a significantly higher response to 1 ppm of acetone, with a response rate of $R_a/R_g = 10.4$, compared to other samples. The detection limit of the proposed SnO_2 nanosheets was found to be as low as 200 ppb. The high response to low concentrations of acetone was

attributed to the (101) crystal facet, which is the main reaction surface. The (101) facet allows for the easy formation of a depletion layer due to the highly reactive Sn^{2+}. Additionally, the acetone adsorption energy on this facet is relatively lower than on other facets. The SnO_2 nanosheet sensor exhibited good selectivity for acetone over other gases like acetaldehyde, isoprene, xylene, toluene, and ammonia [66].

To improve the sensing performance of the SnO_2 based sensors several strategies have been proposed. Among them, the incorporation of Nobel metals [67–69], two dimensional materials [70–72] and catalytic materials [50, 73–75] were received considerable attention. To date, various research efforts have been proposed to demonstrate the result of several key mechanisms involving in the enhancement of gas sensor performance through the incorporation of catalytic materials, including noble metals (such as Au, Pd, Ru), two-dimensional (2D) materials like reduced graphene oxide (rGO) and MXene, and metal oxide heterostructures. Noble metals like Au, Pd, and Ru act as catalytic sites, facilitating the adsorption and reaction of gas molecules on the sensor surface. This leads to a more pronounced change in resistance or capacitance upon exposure to target gases, enhancing sensitivity. These metals can dissociate gas molecules (like O_2) into more reactive atoms, which then 'spillover' onto the sensing material, increasing the rate of reaction with the target gas. Besides, the Noble metals can induce charge transfer to the semiconductor material (like metal oxides), altering its electronic properties and thereby improving its gas sensing response. The incorporation of two-dimensional materials (rGO, MXene) (2D) provides a high surface-to-volume ratio, offering more active sites for gas adsorption. They exhibit high electron mobility, which can enhance the transfer and circulation of charge carriers in the presence of gas molecules, improving the response time and sensitivity. 2D materials can be easily functionalized with other molecules or materials to tailor their sensing properties specifically for certain gases. The formation of metal oxide heterostructures also found to be increase the sensitivity through the interface effect. At the interface of two different metal oxides, electronic and chemical properties can be significantly different from the bulk material, leading to enhanced sensitivity. The alignment of energy bands at the junction can facilitate charge transfer and improve the catalytic efficiency, enhancing the sensor's performance. Different metal oxides can offer complementary sensing mechanisms, which, when combined in a heterostructure, can significantly improve selectivity and sensitivity.

For instance, Xu et al. proposed highly sensitive VOCs-acetone sensor based on Ag-decorated SnO_2 hollow nanofibers for acetone sensing. The Ag-decorated SnO_2 hollow nanofibers were synthesized using an electrospinning technique followed by a silver nitrate treatment. The Ag-decorated SnO_2 sensor exhibited a high response to acetone vapor, with the ability to detect as low as 5 ppm of acetone at 160°C. The sensor's response and recovery times to 50 ppm acetone were approximately 6 s and 10 s, respectively. The sensor showed excellent selectivity towards acetone over other reducing gases such as ethanol, acetic acid, and ammonia. The decoration of SnO_2 hollow nanofibers with silver significantly improved the gas sensing properties. The presence of Ag likely enhances the catalytic oxidation of acetone, leading to an increased sensor response. Besides, the interaction between p-type Ag_2O and n-type SnO_2 in the Ag-decorated SnO_2 nanofibers formed p-n heterojunctions. These heterojunctions are highly sensitive to reducing gases and contribute to the improvement in sensing performance. The addition of Ag also modifies the electrical properties of the SnO_2 nanofibers. It is suggested that the formation of Ag_2O and the interaction with SnO_2 could lead to a more pronounced electron-depleted layer, enhancing the sensor's sensitivity [46]. In another study, Chen et al., proposed highly sensitive acetone sensors based on Y-doped SnO_2 prismatic hollow nanofibers. The prepared SnO_2 prismatic hollow nanofibers were characterized by SEM, TEM, BET, and XPS, revealing a hollow nanostructure with a rough, porous surface, diameters in the range of 154–200 nm, and mesoporous texture. The optimal operating temperature for detecting acetone was found to be 300 ℃. The Y-doped SnO_2 nanofibers exhibited a much higher response to acetone vapor than pure SnO_2, with the 0.4 wt% Y-doped fibers showing the highest response of approximately 174 to 500 ppm acetone. This response was about 7.7 times larger than that of pure SnO_2 hollow nanofibers. The sensor displayed response values of about 12, 60, and 174 for 50, 200, and 500 ppm acetone, respectively. The response and recovery times ranged from 9–30 s to 6–9 s, respectively, across different acetone concentrations. The sensor could detect acetone concentrations as low as 20 ppm, and its response linearly increased with acetone concentration up to 400 ppm. The 0.4 wt% Y-doped SnO_2 nanofibers showed excellent selectivity towards acetone over other gases such as ethanol, dimethylformamide, acetic acid, methanol, and ammonia. The response to acetone was significantly higher, being almost double that to ethanol and eight times higher than to dimethylformamide. The sensor also demonstrated good long-term stability, maintaining nearly constant signals over 60 days of testing at 500 ppm acetone [76]. The Europium (Eu)-doped SnO_2 were proposed as a highly sensitive acetone sensor. Undoped and Eu-doped SnO_2 nanofibers were synthesized using an electrospinning technique and subsequent calcination.

The crystal structure and morphological analysis showed that the nanofibers comprised crystallite grains with an average size of about 10 nm, and Eu ions were successfully doped into the SnO_2 lattice. Compared to pure SnO_2 nanofibers, Eu-doped SnO_2 nanofibers demonstrated significantly enhanced sensing characteristics towards acetone vapor. The sensor based on 2 mol% Eu-doped SnO_2 nanofibers showed the highest response (32.2 for 100 ppm acetone), which was two times higher than that of the pure SnO_2 sensor at an operating temperature of 280 ℃. These sensors also exhibited good sensitivity to acetone in sub-ppm concentrations, with a detection limit extending down to 0.3 ppm. For pure SnO_2 sensors, the maximum response to 100 ppm acetone occurred at 300 ℃. However, for Eu-doped SnO_2 nanofiber sensors, the maximum responses appeared at 280 ℃. The responses of both pure and Eu-doped SnO_2 nanofibers increased linearly with the increase of acetone concentration in the range of 10–500 ppm. Above 1000 ppm, the response rate slowed down, indicating that the sensors became saturated at higher concentrations. The sensors based on Eu-doped SnO_2 nanofibers, especially the 2 mol% Eu-doped SnO_2 sensor, exhibited much higher responses to acetone than to other tested gases, such as ethanol, methanol, acetic acid, DMF, and ammonia [50]. In another study Hu et al., proposed hollow mesoporous SnO_2/Zn_2SnO_4 heterojunction and rGO decoration as a high-performance detection of acetone. The rGO-decorated hollow mesoporous SnO_2/Zn_2SnO_4 composites were synthesized using a self-sacrificial template strategy and acid-assisted etching method. The detailed materials analysis revealed a hollow mesoporous architecture that provides a large specific surface area, enhancing reaction active sites significantly. Compared to solid SnO_2/Zn_2SnO_4 composites, the hollow mesoporous structure of SnO_2/Zn_2SnO_4 sensing materials displayed a higher specific surface area, more internal space, and abundant channel structure. This effectively increased reaction active sites and accelerated the gas penetration and diffusion process, significantly enhancing the sensing performance towards acetone gas. The introduction of rGO into SnO_2/Zn_2SnO_4 was also a critical factor in enhancing gas-sensing performance by offering additional electron migration paths and facilitating electron transfer between oxide semiconductors. The gas-sensitive properties of SnO_2/Zn_2SnO_4-based composites were investigated, including sensitivity, selectivity, and long-term stability. Selectivity tests for rGO-HM-SnO_2/Zn_2SnO_4 and other SnO_2/Zn_2SnO_4 composites were performed against various gases like acetone, ammonia, formaldehyde, methanol, toluene, ethanol, trimethylamine, and xylene at 200 ℃. The rGO-HM-SnO_2/Zn_2SnO_4 sensor displayed the highest response towards acetone, being 10 times higher than responses to other disturbing gases. This excellent selectivity can be attributed to the larger dipole moment of acetone molecules, which makes them easier to be adsorbed on the surface of the sensing materials, and their lower bond dissociation energy, which facilitates interaction with adsorbed oxygen species [77]. SnO-SnO_2 modified two-dimensional MXene Ti_3C_2Tx proposed as a room temperature acetone sensor. In this work the author successfully synthesized a nanocomposite combining SnO-SnO_2 (p–n junction) and Ti_3C_2Tx MXene through a one-step hydrothermal method. The SnO-SnO_2/Ti_3C_2Tx sensor exhibited a significantly improved gas sensing response to acetone at room temperature, with a response value of 12.1, which was nearly 11 and 4 times higher than those of pristine Ti_3C_2Tx and pristine SnO-SnO_2, respectively. The sensor also demonstrated a short recovery time of 9 s and outstanding reproducibility. The selectivity of the SnO-$SnO_2/Ti_3C_2T_x$ sensor was evaluated against other VOCs like ethanol, methanol, and toluene at concentrations ranging from 10 to 100 ppm. The SnO-SnO_2/Ti_3C_2Tx sensor showed significantly higher responsiveness to acetone compared to other VOC gases, indicating its high selectivity for acetone. The response to acetone was 3.4 times higher than that to methanol at 100 ppm, demonstrating its capability as a highly selective acetone gas sensing material. The sensing mechanism of the SnO-$SnO_2/Ti_3C_2T_x$ sensor is based on the gas adsorption/desorption process that leads to variations in electrical resistance. The presence of the p–n junction and the high conductivity of the metallic phase of $Ti_3C_2T_x$ MXene in the SnO-$SnO_2/Ti_3C_2T_x$ sensor contributes to its enhanced sensing performance [78].

The bare SnO_2 and terbium-doped SnO_2 yolk-shell spheres were synthesized through one-pot ultrasonic spray pyrolysis as shown in Fig. 1i [79]. Their acetone sensing characteristics were tested in both dry and wet atmospheres, with relative humidity ranging from 20 to 80%. The bare SnO_2 sensor, despite showing high response and selectivity to acetone, experienced significant deterioration in gas response and sensor resistance in the presence of humidity due to a water poisoning reaction. Conversely, the 5 Tb-SnO_2 sensor was minimally affected by humidity, maintaining its gas response and sensor resistance. The 5 Tb-SnO_2 sensor demonstrated a high response to acetone at 50 ppp with minimal cross-responses to other interfering gases (Fig. 1ii). The humidity-independent gas sensing characteristics were attributed to the maintenance of the concentration of adsorbed oxygen species on the SnO_2 surface, facilitated by the regenerative surface refreshing effect of the Tb^{3+}/Tb^{4+} redox couple and surface OH groups (or water vapor). The proposed sensor is highly sensitive, selective,

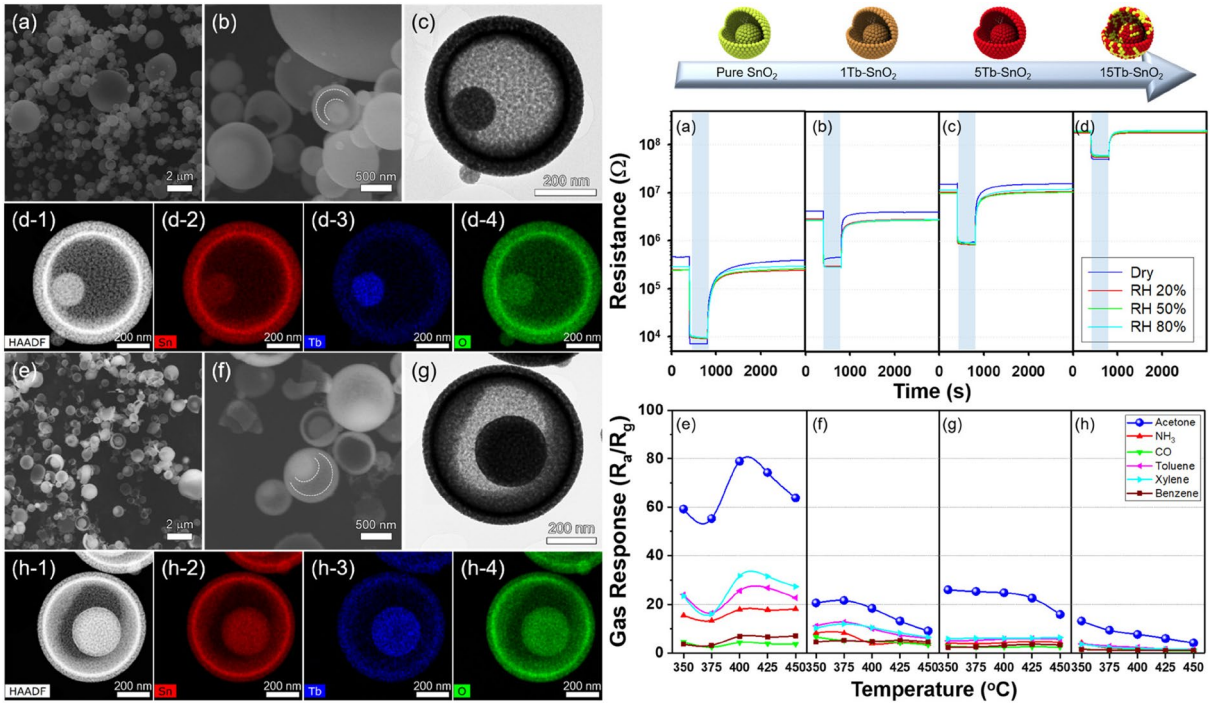

Fig. 1 (i) **a**–**c** Morphological analysis of the 5 Tb–SnO_2 yolk–shell spheres; **d** EDS elemental mapping of Sn, Tb, and O in 5 Tb–SnO_2; **e**–**g** SEM and TEM images of 15 Tb–SnO_2; and **h** EDS elemental mapping of Sn, Tb, and O in 15 Tb–SnO_2. (ii) Gas sensing transients of the (**a**) pure SnO_2, (**b**) 1 Tb–SnO_2, (**c**) 5 Tb–SnO_2, and (**d**) 15 Tb–SnO_2 sensors to 20 ppm of acetone at 450 ℃ under dry and humid conditions (RH = 20, 50, 80%). Gas responses of (**e**) pure SnO_2, (**f**) 1 Tb–SnO_2, (**g**) 5 Tb–SnO_2, and (**h**) 15 Tb–SnO_2 sensors to various gases (concentration: 20 ppm) at 350, 375, 400, 425, and 450 ℃ under dry condition. Reprinted from [79] with permission from American Chemical Society Copyright (2018) American Chemical

and unaffected by humidity, which are suitable for the miniaturized and real-time analysis of exhaled breath for the diagnosis of diabetes. In another study hierarchically assembled with bimodal pore-loaded hierarchical SnO_2 spheres (PH-SnO_2) were successfully synthesized through an electrostatic spraying method combined with a colloidal templating route using polystyrene beads.

These hierarchical SnO_2 spheres show enhanced gas sensing performance due to their high porosity. The synthesized porous SnO_2 spheres were used as sensing layers for the detection of acetone and exhibited about a 20% enhanced response compared to hierarchical SnO_2 (H-SnO_2) spheres without pores. The Pt-functionalized PH-SnO_2 (Pt-PH-SnO_2) spheres demonstrated significantly improved acetone detection capabilities, showing a response of 44.83 at 5 ppm compared to PH-SnO_2 spheres with a response of 6.61, as well as superior selectivity (Fig. 2) [80]. The principal component analysis (PCA), of dense SnO_2 spheres, PH-SnO_2 spheres, and Pt-PH-SnO_2 spheres distinguished between four distinct gases, including acetone, toluene, hydrogen sulfide, and ammonia, at concentrations varying from 1 to 5 ppm, with clear separation between them as shown in Fig. 2c.

Jang et al. proposed a Highly Porous SnO_2 nanotubes functionalized with biomimetic nanocatalysts for direct observation of simulated diabetes [81]. This route combines Oswald-ripening driven single-nozzle electrospinning with a sacrificial templating route including polymeric colloids and protein-templated catalysts in solution. The resulting sensor arrays can clearly distinguish the breath samples of healthy individuals from those simulating diabetic conditions, showing potential as diagnostic tools for diabetes through exhaled breath tests. The sensors have been optimized for acetone sensing performance by adjusting the Pt catalyst content, indicating that well-dispersed and sub-nanoscale catalytic nanoparticles can enhance sensing performance. The best sensing performances were observed with 0.08 wt% Pt catalyst loaded porous SnO_2 NTs. E-nose sensor arrays assembled with three different sensing layers were able to differentiate between simulated diabetic breath and healthy breath in the presence of interfering gases.

This innovation holds potential not only in health care for the diagnosis of diabetes but also in environmental monitoring applications. As shown in Fig. 3, PCA of the obtained sensor data indicates that distinction between

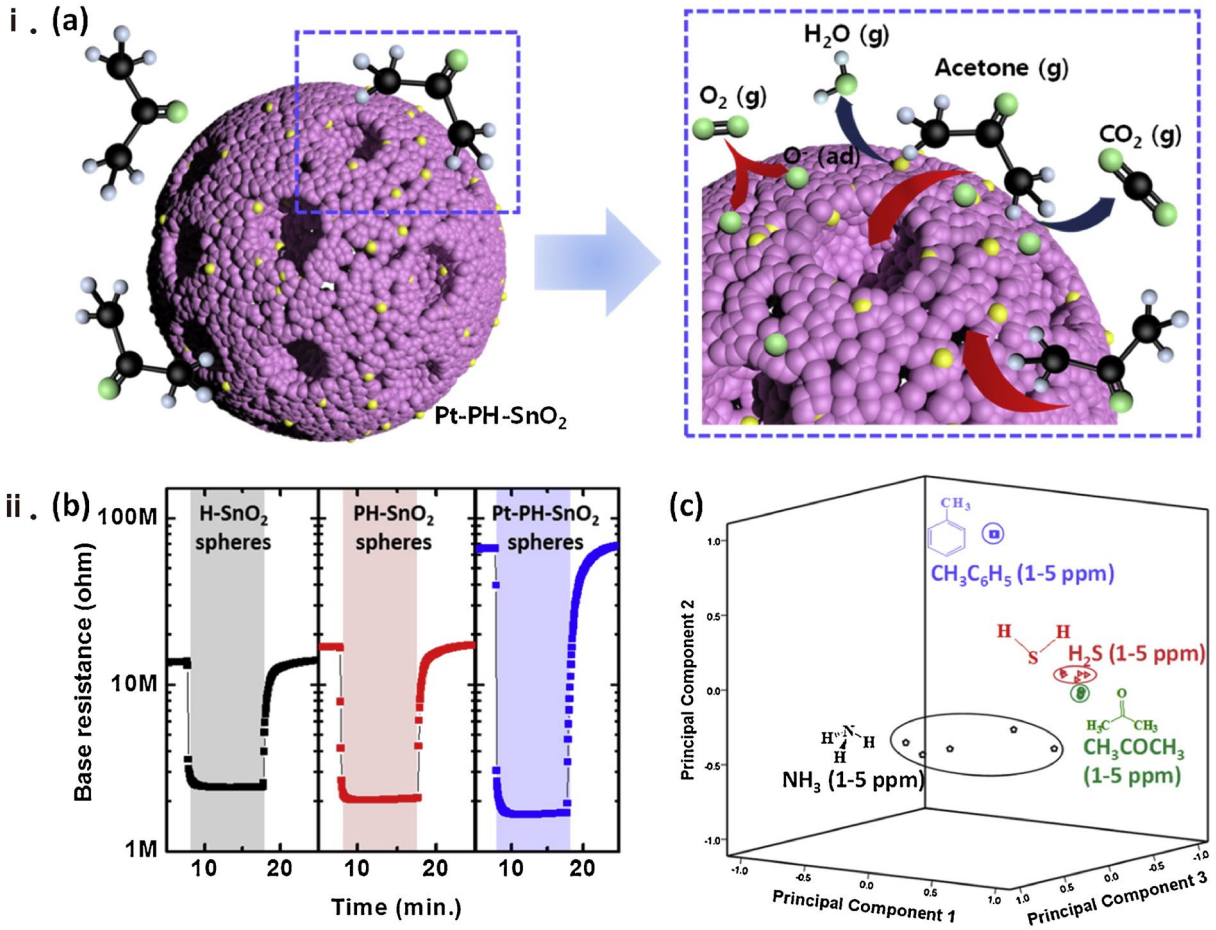

Fig. 2 **a** Schematic images of acetone sensing mechanism of Pt-PH-SnO_2 spheres, **b** base resistances of dense SnO_2 spheres, PH-SnO_2 spheres, and Pt-PH-SnO_2 spheres, and (**c**) pattern recognition using principal component analysis (PCA) of simulated gases (1–5 ppm) with dense SnO_2 spheres, PH-SnO_2 spheres, and Pt-PH-SnO_2 spheres-based sensors. Reprinted from [80] with permission from Elsevier Copyright (2020) Elsevier

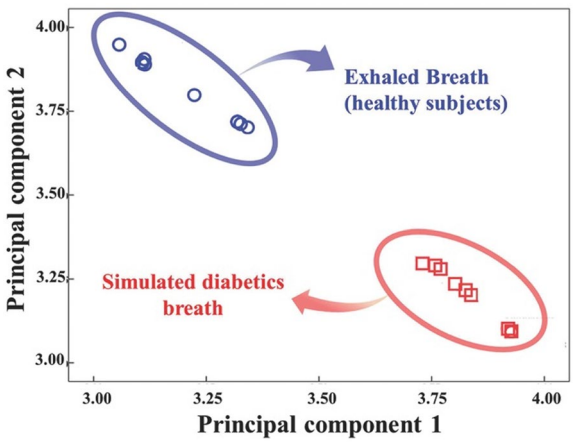

Fig. 3 Pattern recognition based on PCA using sensor arrays (PS-SnO_2 NTs, Pt-PS-SnO_2 NTs, and Pt-SnO_2 NTs). Reprinted from [81] with permission from John Wiley and Sons Copyright (2016) John Wiley and Sons

the simulated diabetics breath and healthy people's breath was clearly observed. 10 people exhaled breath samples and 10 simulated diabetic breath samples were categorized to two distinguishable clusters without any overlap. This result demonstrates that the outstanding sensor arrays using Pt-PS-SnO_2 NTs, Pt-SnO_2 NTs, and PS-SnO_2 NTs with outstanding sensing properties have high potential for diagnosis of diabetes. Table 2 summarize the acetone sensing characteristics of the SnO_2 based sensors incorporated with catalytic, metal nanoparticles, rGO and other metal oxide nanostructures.

The heterostructured SnO_2 nanocomposites have been proposed as effective acetone sensors. Figure 4a shows the high-performance acetone gas sensor based on ruthenium (Ru)-doped SnO_2 nanofibers. Kou et al. report on the enhanced gas-sensing properties of SnO_2 nanofibers doped with ruthenium for acetone detection [84]. The study shows that 2 mol% Ru-doped SnO_2 nanofibers have a response 12 times higher to 100 ppm acetone compared

Table 2 Acetone sensing characteristics of the SnO_2-based gas sensors

Materials	Temp (°C)	Conc. (ppm)	Response (s)	Response/recovery times (s)	Ref
PdAu/SnO_2	250	2	6.5	5/4	[82]
Au/ SnO_2	220	5	3.1	0.9/21	[67]
Rh/ SnO_2	200	50	60.6	2/64	[69]
Ru/ SnO_2 hollow nanotubes	250	100	340	0.58/8.4	[83]
Ru/ SnO_2 nanofibers	200	100	118.8	1/86	[84]
$ZnSnO_3$/ZnO Hollow spheres	280	50	17.3	3/13	[85]
Solid SnO_2/$ZnSnO_3$ spheres	290	100	15	12/118	[86]
double-shell hollow SnO_2/$ZnSnO_3$ spheres	290	100	30	9/122	[86]
Ce-SnO_2 nanoparticles	270	50	50.5	17/38	[75]
Co-SnO_2	350	1000	1637	75/-	[87]
SnO_2/ZnO heterostructure	300	100	85	19/9	[88]
SnO_2/Au-doped In_2O_3 core–shell nanofibers	300	100	12	2/9	[89]
SnO_2-rGO	35	10	2.19	107/146	[90]
Pt-SnO_2 nanofibers	170	100	104.26	107/90	[91]
TiO_2/SnO_2 heterostructure	280	100	13.7	2/60	[92]
Pd@ZnO-SnO_2	400	5	10.12	16/36	[93]
Hollow SnO_2 nanobelt	260	5	6.7	38/9	[56]
RGO-SnO_2 NFs	350	5	10.0	28/100	[51]
Pt-SnO_2 NFs	400	3	7.12	30/20	[94]
Pt-SnO_2 NTs	350	1	25	40/60	[95]
Pt-PS_SnO_2 NTs	350	1	34.8	-/-	[63]

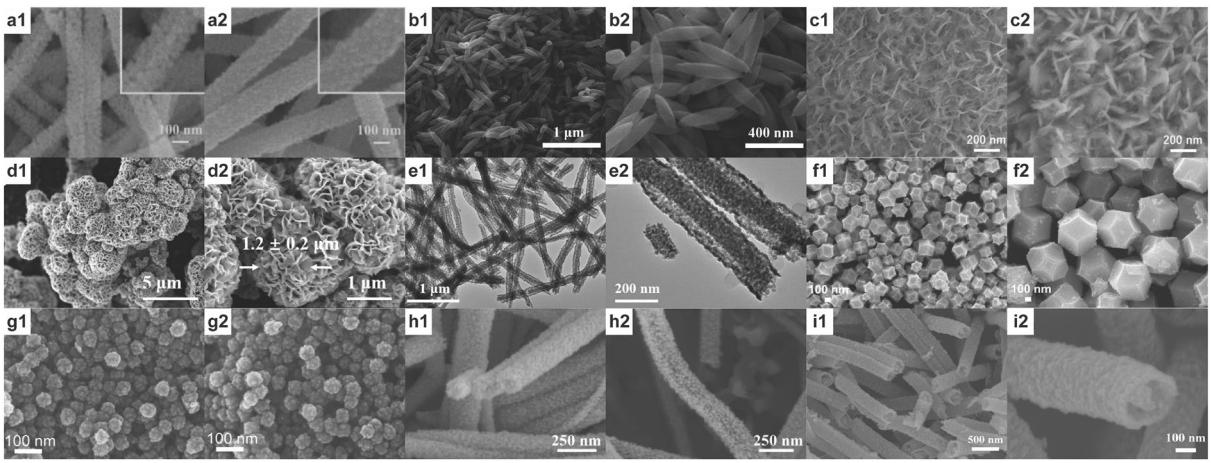

Fig. 4 Various nanostructures-based acetone sensors. (a1, a2) Ruthenium (Ru)-doped SnO_2 nanofibers [Reprinted from [84] with permission from Elsevier. Copyright (2020) Elsevier]. (b1, b2) Hierarchical assembly of SnO_2 nanorods on spindle-like α-Fe_2O_3 [Reprinted from [49] with permission from Elsevier. Copyright (2021) Elsevier]. (c1, c2) Catalyst-free highly sensitive SnO_2 nanosheet [Reprinted from [66] with permission from American Chemical Society. Copyright (2020) American Chemical.]. (d1, d2) α-Fe_2O3/SnO_2 nanoball arrays [Reprinted from [96] with permission from John Wiley and Sons. Copyright (2020) John Wiley and Sons.]. (e1, e2) Co_3O_4/SnO_2 yolk-shell nanofibers [Reprinted from [34] with permission from Elsevier. Copyright (2024) Elsevier]. (f1, f2) metal–organic framework-derived SnO_2-ZnO [Reprinted from [37] with permission from Elsevier. Copyright (2023) Elsevier]. (g1, g2) Co-catalyzed SnO_2 nanospheres [Reprinted from [73] with permission from Elsevier. Copyright (2020) Elsevier]. (h1, h2) Pt catalyst decorated SnO_2 porous nanofibers [Reprinted from [91] with permission from Elsevier. Copyright (2022) Elsevier] and (i1, i2) hollow hierarchical TiO_2-SnO_2-TiO_2 composite nanofibers Reprinted from [47] with permission from Elsevier Copyright (2021) Elsevier

to pure SnO_2 nanofibers. The enhanced sensing response of the proposed sensor is attributed to improvements in gas sensing performance due to changes in electron concentration and oxygen component distribution from Ru incorporation. Liu et al. proposed a hierarchical assembly of SnO_2 nanorods on spindle-like α-Fe_2O_3 for enhanced acetone gas-sensing performance (Fig. 4b) [49]. The study reveals that SnO_2-functionalized Fe_2O_3 heterostructure nanospindles exhibit enhanced sensitivity and selectivity for acetone gas detection compared to pure Fe_2O_3, demonstrating approximately 4.3 times greater sensitivity to acetone at an optimal working temperature of 280 ℃. The response and recovery times for these sensors are also rapid, significantly improving the practical utility of the proposed sensor. Kim et al. proposed catalyst-free highly sensitive SnO_2 nanosheet gas sensors for trace-level detection of acetone (Fig. 4c) [66]. Wang et al. demonstrate the construction of hierarchical α-Fe_2O3/SnO_2 nanoball arrays with superior acetone sensing performance (Fig. 4d) [96]. The α-Fe_2O_3/SnO_2 nanoball arrays exhibit superior sensing performance compared to pure SnO_2 [34]. The α-Fe_2O_3/SnO_2 sensor shows notable sensitivity, selectivity, and a wide detection range for acetone, making it highly effective for detecting low acetone concentrations. The enhanced performance is attributed to the hierarchical nanostructure and the synergistic effect of the α-Fe_2O_3/SnO_2 composition. In another study, the construction of Co_3O_4/SnO_2 yolk-shell nanofibers for acetone gas detection presents significant findings in gas sensor technology (Fig. 4e) [37]. The Co_3O_4/SnO_2 yolk-shell nanofibers exhibit an outstanding response of approximately 216 to 100 ppm acetone at 350 ℃, coupled with an ultrafast response time of about 0.62 s. The sensors demonstrate remarkable selectivity for acetone and excellent stability in both humidity and long-term use. Other exotic nanostructures based on metal–organic framework-derived SnO_2-ZnO (Fig. 4f), Co-catalyzed SnO_2 nanospheres (Fig. 4g) [73], Pt catalyst-decorated SnO_2 porous nanofibers (Fig. 4h) [91], and hollow hierarchical TiO_2-SnO_2-TiO_2 composite nanofibers (Fig. 4i) [47] with increased active-sites and charge transfer have also been proposed as effective acetone sensors. These findings demonstrate the potential of using such heterostructures and composite materials in developing effective acetone sensors for various applications.

Other metal oxide semiconductor-based acetone sensors with enhanced sensing characteristics along with fast response and recover time also reported. Among them, WO_3 and ZnO has received considerable attention. WO_3 a with a band gap of approximately 2.6 eV, is increasingly recognized in the field of gas sensing technology, particularly for VOCs detection. This recognition is attributed to WO_3's exceptional gas sensing characteristics, its notable electrical properties, and its inherent non-toxicity, making it a viable candidate for environmental and health monitoring applications. WO_3 exhibits a series of stable phase transitions at different temperature ranges, each phase offering distinct advantages for gas detection. Notably, the monoclinic WO_3 phase is the predominant crystal structure in bulk WO_3 at or above ambient temperatures. This has spurred extensive research into this particular phase due to its favorable properties for gas sensor development. A significant body of work in sensor technology has leveraged this monoclinic WO_3 phase to engineer sensors capable of detecting a wide array of gases. However, the orthorhombic WO_3 phase, often denoted as β-WO_3, is especially noteworthy for its acute sensitivity and selectivity in detecting acetone at ppb concentrations. This heightened sensitivity can be largely attributed to the intrinsic electric dipole moment characteristic of the β-phase. This feature enhances the interaction between β-WO_3 and analytes with high dipole moments, such as acetone, thereby amplifying the sensor's response to these specific compounds.

For instance, Kim et al. discusses the acetone sensing characteristics of Apo-Pt@HP WO_3 nanofibers (Fig. 5i). The sensors were tested under various operating temperatures (300–450 ℃) and different loading concentrations of Apo-Pt nanoparticles in a highly humid atmosphere (90% RH). The sensor functionalized with 0.05 wt% Apo-Pt NPs exhibited the highest response at a lower temperature of 350 ℃ due to the catalytic action of the Pt, which reduced the activation energy required for the surface reaction. The 0.05 wt% Apo-Pt@HP WO_3 NFs showed a high response ($R_a/R_g = 88.04 \pm 3.18$) at 5 ppm of acetone, significantly outperforming other sensors and demonstrating a 15.9-fold to 26.4-fold improvement [97]. The minimum detectable concentration for these NFs was 0.4 ppm with a response of 2.1. Additionally, these NFs exhibited remarkable selectivity towards 5 ppm acetone when compared to other interfering gases such as hydrogen sulfide, toluene, ethanol, carbon monoxide, ammonia, and methane at 350 ℃. The improved acetone sensing properties are attributed to structural and catalytic effects, such as an increased surface-to-volume ratio and hierarchical interconnectivity of porosity. Furthermore, the Apo-Pt@HP WO_3 NFs showed excellent acetone selectivity confirmed by PCA, which clustered acetone molecules distinctly from other biomarkers, indicating the potential of these sensors for non-invasive breath sensor platforms for selective detection of specific biomarker molecules (Fig. 5ii). Sensors fabricated from WO_3 nanosheets and g-C_3N_4/WO_3 composites were tested at various temperatures to determine the optimal operating temperature [98]. It was observed that the 1 wt% g-C_3N_4/WO_3 sensor exhibited a maximum response of 35 to

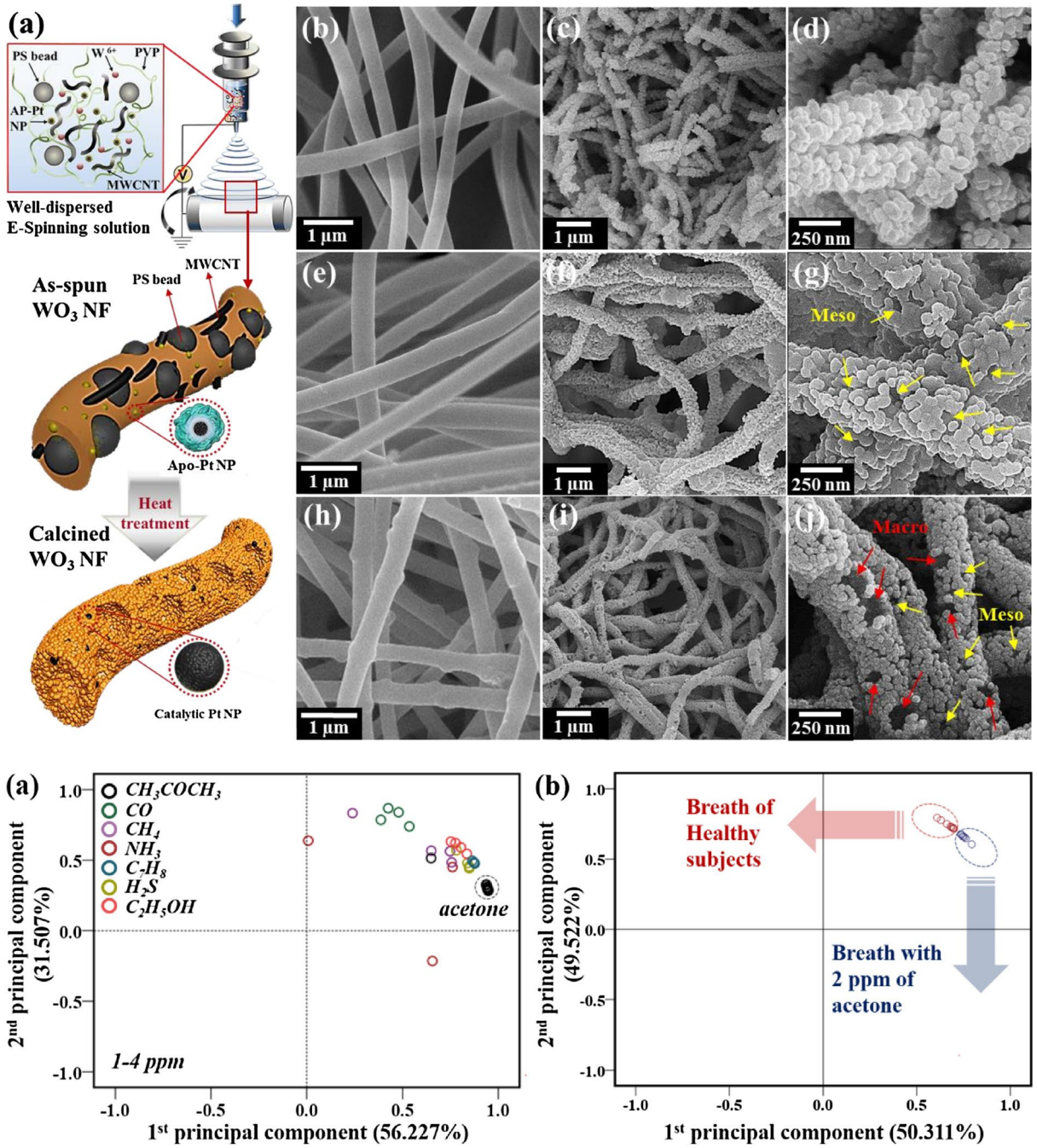

Fig. 5 (i) Schematic illustration of the sacrificial templates assisted electrospinning fabrication process for hierarchically porous WO_3 NFs functionalized by Apo-Pt NPs, SEM images of (**b**-**i**) as-spun W precursor/PVP composite NFs, (**c**) dense WO_3 NFs after calcination, and (**d**) magnified image of (**c**), SEM images of (**e**) as-spun W precursor/PVP composite NFs embedded with MWCNTs, (**f**) MP_WO_3 NFs after calcination, and (**g**) magnified image of (**f**). SEM images of (**h**) as-spun W precursor/PVP composite NFs embedded with MWCNTs, PS colloids and Apo-Pt NPs, (**i**) Apo-Pt@HP_WO_3 NFs after calcination, and (**j**) magnified image of (i). (ii) Pattern recognition based on principal component analysis (PCA) using sensor arrays (Apo-Pt@HP_WO_3 NFs, HP_WO_3 NFs and MP_WO_3 NFs) for (**a**) selectivity and (**b**) diagnosis of simulated acetone breath. Reprinted from [97] with permission from Elsevier Copyright (2018) Elsevier

100 ppm acetone at 340 ℃, which is about three times higher than that of WO_3 nanosheets at the same temperature, indicating that g-C_3N_4/WO_3 materials enhance acetone detection performance. The g-C_3N_4/WO_3 composites demonstrated better selectivity compared to other loading amounts, with the 1 wt% g-C_3N_4/WO_3

sensor exhibiting at least seven times higher response to acetone than to other interfering gases, which could be attributed to the ε-phase WO_3 in the composite having a strong interaction with polar acetone molecules. The response and recovery times for sensors based on WO_3 nanosheets and g-C_3N_4/WO_3 composites were around 5 s. Li et al. have employed ruthenium (Ru)-loaded WO_3 nanoparticles to detect acetone vapor. The acetone sensing response manifested by the Ru-loaded WO_3 sensors was significantly augmented compared to that of pristine WO_3, achieving a markedly reduced detection threshold as low as 0.5 ppm. Notably, a 1 wt% Ru loading on WO_3 demonstrated the most pronounced response, achieving a resistance ratio (R_a/R_g) of approximately 7.3 at an operational temperature of 300 ℃ for the detection of 1.5 ppm acetone vapor [99]. Chen et al. investigated the gas sensing properties of WO_3/Pt-decorated rGO nanocomposite sensors. They reported that the sensor exhibited a maximum response of 12.2 upon exposure to 10 ppm of acetone vapor at an operating temperature of 200 ℃ [100]. Shen et al. synthesized iron and carbon co-doped WO_3 with a hierarchical walnut-like morphology to enhance selectivity for acetone vapor detection. The resulting sensor demonstrated an enhanced response ratio (R_a/R_g) of approximately 17 at an operating temperature of 300 ℃ when exposed to 10 ppm of acetone in a configuration where the doping ratio of Fe to WO_3 was 0.992 atomic percent (at1%) [101]. Righettoni et al. fabricated the chemosensors using synthesized pure and Si-doped WO_3 nanoparticles, aiming to perform quantitative analysis of acetone under dry air and 90% RH conditions. The sensor's response to ppb of acetone at a temperature of 400 ℃ in dry air was recorded as 4.63, which was significantly higher compared to its response (0.7) to 90% RH. Nevertheless, an increase in relative humidity to 90% led to a reduction in the sensor's response, falling to 68% of the response observed for 600 ppb acetone in dry air. This observation signifies the substantial impact of humidity in diminishing the sensor's sensitivity. Despite this, the sensor exhibited a rapid response capability to acetone concentrations as low as 20 ppb even under high RH conditions [102].

ZnO is yet another favored metal oxide in gas detection research. For instance, Wang et al., proposed ZnO nanosheets incorporated graphene oxide nanocomposites for highly effective acetone vapor detection. Compared to undoped ZnO nanostructures and ZnO nanosheets alone, the ZnO/GO nanocomposite sensor exhibited enhanced gas response, faster response-recovery times, and improved selectivity. The optimal operating temperature for the sensor was determined to be 240 ℃. Additionally, the ideal mass fraction of GO in the ZnO/GO nanocomposites was found to be 10 wt%. Under these optimized conditions, the ZnO/GO nanocomposites sensor achieved a response value of 35.8 to 100 ppm of acetone. The superior sensing properties of the nanocomposites are attributed to their unique 2D–2D composite structure, combining the rigidity of ZnO with the flexibility of GO. The 2D morphology of the nanocomposites contributes to a large effective surface area, which significantly enhances the sensor's response. Additionally, the rich functional groups in GO aid in the adsorption of gases, further improving the sensor's performance [103]. Hierarchically structured ZnO spheres were prepared via a solvothermal technique. The dandelion-mimicking ZnO spheres exhibited a response of 33 toward 100 ppm acetone at 300 ℃. The response time of the sensor was found to be 3 s. The gas detector also exhibited a pronounced selectivity towards acetone. Such high selectivity correlated with acetone's prominent dipole moment (2.88 D) in relation to other gases, enhancing its adhesion potential on ZnO's polar (002) facets, resulting in robust selectivity for acetone [104]. In another study, the ZnO nanorod thin films on pre-deposited SiO_2/ Si substrates were proposed for acetone sensing. The ZnO nanorod-based sensor exhibited excellent sensing performance for acetone at an operating temperature of 300 ℃. The sensor demonstrated the ability to detect acetone concentrations as low as 1 ppm. The response time of the sensor was approximately 5 s, and the recovery time was about 15 s. Porous Pt-doped In_2O_3 NFs based sensors were used for acetone sensing. This increased surface area, combined with the catalytic properties of Pt, facilitates the formation of Pt-In_2O_3 Schottky barriers. These features, in conjunction with the nanofibers' porous architecture, enabled the sensitive detection of acetone gas concentrations as low as 10 ppb at 180 ℃. The sensor demonstrated rapid gas sensing kinetics, evidenced by swift response and recovery times of 6 s and 9 s, respectively [105]. Similarly other exotic nanostructures based on TiO_2 [106], Co_3O_4 [107], NiO [108], Fe_2O_3 [109], etc. also have been proposed for the acetone sensing analysis.

Limitation of the nanostructures-based breath sensors

Nanostructure-based breath sensors, employed extensively for biomarker detection in medical diagnostics and other applications, encounter numerous scientific challenges. An important issue is the discrimination of target gas molecules amidst a complex milieu of other gases in human breath, such as water vapor, carbon dioxide, and various VOCs, which can confound the detection of specific biomarkers. The attainment of high sensitivity is critical, particularly at low target gas concentrations, to ensure precise diagnoses. Certain disease markers

exist at exceptionally low concentrations, necessitating the capability of sensors to discern gas levels in the ppb range or even at parts-per-trillion (ppt). Moreover, managing humidity levels presents a significant obstacle, given the substantial moisture content in human breath. The prevalent water vapor can markedly impact the efficacy of metal oxide sensors, typically resulting in diminished sensitivity and selectivity. The long-term stability and repeatability of these sensors are vital for dependable diagnoses. Over time, metal oxide sensors are prone to response drift due to aging, thermal fluctuations, and exposure to diverse gases. Many metal oxide sensors necessitate operation at elevated temperatures to function optimally, which can increase power consumption, potentially rendering them less suitable for portable or wearable devices. The propensity of these sensors to react to multiple gases introduces issues of cross-sensitivity, where responses to non-target gases could impede accurate target gas detection. Developing compact, portable, and integrated systems that retain high performance is an arduous but necessary task for their practical and broad application. Fabricating high-quality, consistent, and cost-effective sensors is imperative for their commercial success, particularly in contexts requiring disposable or single-use breath analysis tools. Furthermore, compliance with health and safety standards, especially in medical diagnostics, is crucial. This encompasses considerations of biocompatibility and non-invasiveness. To surmount these challenges, ongoing research in materials science, nano-engineering, and signal processing is being pursued, aiming to amplify the performance and utility of metal oxide-based breath sensors across various domains.

Conclusion

The exploration of metal oxide-based breath sensors reveals a promising yet challenging landscape in the realm of gas sensing technology, particularly for medical diagnostics. These sensors, leveraging the properties of materials like SnO_2, WO_3, ZnO, In_2O_3, etc. have shown significant potential in detecting biomarkers in human breath, crucial for diagnosing various health conditions. Innovations such as doping with various materials have enhanced their sensitivity and selectivity, crucial for detecting acetone at very low-concentration compounds. Key achievements in this field include the successful synthesis of high-surface-area nanocomposites, the ability to operate at lower temperatures, and improvements in response and recovery times. These advances address some of the fundamental challenges such as selectivity in complex gas mixtures, sensitivity at low concentrations, and the influence of humidity. The future of nanostructure based breath sensors lies in further improving sensitivity, selectivity, and stability. Research is ongoing to develop sensors that can detect low concentrations of gases with high accuracy and in complex environments. The integration of artificial intelligence for data analysis and the exploration of new materials and fabrication techniques continue to drive the field forward.

Outlook

Looking forward, the field of nanostructured-based breath sensors is poised for significant advancements, although key challenges remain. Continuous efforts are needed to further improve the selectivity and sensitivity of these sensors, especially in the presence of complex gas mixtures and varying humidity levels. The integration of advanced materials, like graphene and other 2D materials, could offer new pathways to overcome these challenges. Miniaturization and integration into portable devices remain crucial for the widespread application of these sensors, especially in personal healthcare and real-time monitoring. The development of low-cost, high-performance sensors compatible with portable electronics will be a significant step towards this goal. In the realm of manufacturing and commercialization, achieving consistency in sensor production and maintaining low costs are essential for broader adoption. Additionally, ensuring compliance with health and safety standards, particularly in medical applications, will remain a priority. From a research perspective, the exploration of novel materials and nano-engineering techniques holds promise. The application of machine learning and advanced signal processing methods could further enhance the performance and applicability of these sensors. The integration of sensor technology with wireless communication and IoT devices opens new frontiers for real-time health monitoring and environmental sensing. In conclusion, nanostructure-based breath sensors have already shown substantial promise in medical diagnostics and environmental monitoring. With ongoing research and technological advancements, these sensors are set to play a pivotal role in the future of healthcare and smart sensing technologies.

Acknowledgements

Authors are grateful to the National Research Foundation of Korea for the funds received.

Author contributions

AS: Conceptualization, figure preparation, writing—original manuscript and discusses with MK; DWL: Supervision, funding acquisition, writing—review. All authors read and approved the final manuscript.

Funding

This work was financially supported by the National Research Foundation of Korea (NRF) grant funded by the Korean government (MSIT) (No. 2020R1A5A8018367) and Basic Science Research Program through the

National Research Foundation of Korea (NRF) funded by the Ministry of Education (RS-2023-00250781).

Availability of data and materials
The datasets supporting the conclusions of this article are included within the article.

Declarations

Ethics approval and consent to participate
Not applicable.

Consent for publication
Not applicable.

Competing interests
The authors declare that they have no competing interests.

Received: 22 November 2023 Accepted: 17 December 2023
Published online: 04 January 2024

References

1. Drabińska N, Flynn C, Ratcliffe N, Belluomo I, Myridakis A, Gould O, Fois M, Smart A, Devine T, Costello BD (2021) A literature survey of all volatiles from healthy human breath and bodily fluids: the human volatilome. J Breath Res 15(3):034001. https://doi.org/10.1088/1752-7163/abf1d0
2. Sun X, He J, Yang X (2017) Human breath as a source of VOCs in the built environment, Part I: a method for sampling and detection species. Build Environ 125:565–573. https://doi.org/10.1016/j.buildenv.2017.06.038
3. Hakim M, Broza YY, Barash O, Peled N, Phillips M, Amann A, Haick H (2012) Volatile organic compounds of lung cancer and possible biochemical pathways. Chem Rev 112(11):5949–5966. https://doi.org/10.1021/cr300174a
4. Rudnicka J, Walczak M, Kowalkowski T, Jezierski T, Buszewski B (2014) Determination of volatile organic compounds as potential markers of lung cancer by gas chromatography–mass spectrometry versus trained dogs. Sens Actuators B Chem 202:615–621. https://doi.org/10.1016/j.snb.2014.06.006
5. Buszewski B, Kęsy M, Ligor T, Amann A (2007) Human exhaled air analytics: biomarkers of diseases. Biomed Chromatogr 21(6):553–566. https://doi.org/10.1002/bmc.835
6. Mazzone PJ (2008) Analysis of volatile organic compounds in the exhaled breath for the diagnosis of lung cancer. J Thorac Oncol 3(7):774–780. https://doi.org/10.1097/JTO.0b013e31817c7439
7. Deng C, Zhang J, Yu X, Zhang W, Zhang X (2004) Determination of acetone in human breath by gas chromatography–mass spectrometry and solid-phase microextraction with on-fiber derivatization. J Chromatogr B 810(2):269–275. https://doi.org/10.1016/j.jchromb.2004.08.013
8. Westmoreland DG, Rhodes GR (1989) Analytical techniques for trace organic compounds-II. Detectors for gas chromatography. Pure Appl Chem 61(6):1147–1160. https://doi.org/10.1351/pac198961061147
9. Abbott SM, Elder JB, Španěl P, Smith D (2003) Quantification of acetonitrile in exhaled breath and urinary headspace using selected ion flow tube mass spectrometry. Int J of Mass Spectrom 228(2–3):655–665. https://doi.org/10.1016/S1387-3806(03)00212-4
10. Wehinger A, Schmid A, Mechtcheriakov S, Ledochowski M, Grabmer C, Gastl GA, Amann A (2007) Lung cancer detection by proton transfer reaction mass-spectrometric analysis of human breath gas. Int J of Mass Spectrom 265(1):49–59. https://doi.org/10.1016/j.ijms.2007.05.012
11. Chen X, Cao M, Li Y, Hu W, Wang P, Ying K, Pan H (2005) A study of an electronic nose for detection of lung cancer based on a virtual SAW gas sensors array and imaging recognition method. Meas Sci Technol 16(8):1535. https://doi.org/10.1088/0957-0233/16/8/001
12. Manjula P, Arunkumar S, Manorama SV (2011) Au/SnO_2 an excellent material for room temperature carbon monoxide sensing. Sens Actuators B Chem 152(2):168–175. https://doi.org/10.1016/j.snb.2010.11.059
13. Shanmugasundaram A, Ramireddy B, Basak P, Manorama SV, Srinath S (2014) Hierarchical In $(OH)_3$ as a precursor to mesoporous In_2O_3 nanocubes: a facile synthesis route, mechanism of self-assembly, and enhanced sensing response toward hydrogen. J Phys Chem C 118(13):6909–6921. https://doi.org/10.1021/jp5010659
14. Arunkumar S, Hou T, Kim YB, Choi B, Park SH, Jung S, Lee DW (2017) Au Decorated ZnO hierarchical architectures: facile synthesis, tunable morphology and enhanced CO detection at room temperature. Sens Actuators B Chem 243:990–1001. https://doi.org/10.1016/j.snb.2016.11.152
15. Shanmugasundaram A, Basak P, Satyanarayana L, Manorama SV (2013) Hierarchical SnO/SnO_2 nanocomposites: formation of in situ p–n junctions and enhanced H2 sensing. Sens Actuators B Chem 185:265–273. https://doi.org/10.1016/j.snb.2013.04.097
16. Bruderer T, Gaisl T, Gaugg MT, Nowak N, Streckenbach B, Müller S, Moeller A, Kohler M, Zenobi R (2019) On-line analysis of exhaled breath: focus review. Chem Rev 19(19):10803–10828. https://doi.org/10.1021/acs.chemrev.9b00005
17. Di Natale C, Paolesse R, Martinelli E, Capuano R (2014) Solid-state gas sensors for breath analysis: a review. Anal Chim Acta 824:1–7. https://doi.org/10.1016/j.aca.2014.03.014
18. Hibbard T, Crowley K, Kelly F, Ward F, Holian J, Watson A, Killard AJ (2013) Point of care monitoring of hemodialysis patients with a breath ammonia measurement device based on printed polyaniline nanoparticle sensors. Anal Chem 85(24):12158–12165. https://doi.org/10.1021/ac403472d
19. McQuade DT, Pullen AE, Swager TM (2000) Conjugated polymer-based chemical sensors. Chem Rev 100(7):2537–2574. https://doi.org/10.1021/cr9801014
20. Shao Y, Wang J, Wu H, Liu J, Aksay IA, Lin Y (2010) Graphene based electrochemical sensors and biosensors: a review. Electroanalysis 22(10):1027–1036. https://doi.org/10.1002/elan.200900571
21. Filipiak W, Sponring A, Filipiak A, Ager C, Schubert J, Miekisch W, Amann A, Troppmair J (2010) TD-GC-MS analysis of volatile metabolites of human lung cancer and normal cells in vitro. Cancer Epidemiol Biomarkers Prev 19(1):182–195. https://doi.org/10.1158/1055-9965.EPI-09-0162
22. Sulé-Suso J, Pysanenko A, Španěl P, Smith D (2009) Quantification of acetaldehyde and carbon dioxide in the headspace of malignant and non-malignant lung cells in vitro by SIFT-MS. Analyst 134(12):2419–2425. https://doi.org/10.1039/B916158A
23. Haick H, Broza YY, Mochalski P, Ruzsanyi V, Amann A (2014) Assessment, origin, and implementation of breath volatile cancer markers. Chem Soc Rev 43(5):1423–1449. https://doi.org/10.1039/C3CS60329F
24. Paleczek A, Rydosz A (2022) Review of the algorithms used in exhaled breath analysis for the detection of diabetes. J Breath Res 16(2):026003. https://doi.org/10.1088/1752-7163/ac4916
25. Drmosh QA, Olanrewaju Alade I, Qamar M, Akbar S (2021) Zinc oxide-based acetone gas sensors for breath analysis: a review. Chem Asian J 16(12):1519–1538. https://doi.org/10.1002/asia.202100303
26. Masikini M, Chowdhury M, Nemraoui O (2020) Reorientation of polymers in an applied electric field for electrochemical sensors. J Electrochem Soc 67:03753. https://doi.org/10.1149/1945-7111/ab6cfe
27. Dereziński T, Zozulińska-Ziółkiewicz D, Uruska A, Dąbrowski M (2020) Abdominal aorta diameter as a novel marker of diabetes incidence risk in elderly women. Sci Rep 10:13734. https://doi.org/10.1038/s41598-020-70736-1
28. Shanmugasundaram A, Basak P, Manorama SV, Krishna B, Sanyadanam S (2015) Hierarchical mesoporous In_2O_3 with enhanced CO sensing and photocatalytic performance: distinct morphologies of In $(OH)_3$ via self-assembly coupled in situ solid–solid transformation. ACS Appl Mater Interfaces 7(14):7679–7689. https://doi.org/10.1021/acsami.5b00584
29. Shanmugasundaram A, Chinh ND, Jeong YJ, Hou TF, Kim DS, Kim D, Kim YB, Lee DW (2019) Hierarchical nanohybrids of B-and N-codoped graphene/mesoporous NiO nanodisks: an exciting new material for selective sensing of H_2S at near ambient temperature. J Mater Chem A 7(15):9263–9278. https://doi.org/10.1039/C9TA00755E
30. Shanmugasundaram A, Gundimeda V, Hou T, Lee DW (2017) Realizing synergy between In_2O_3 nanocubes and nitrogen-doped reduced

graphene oxide: an excellent nanocomposite for the selective and sensitive detection of CO at ambient temperatures. ACS Appl Mater Interfaces 9(37):31728–31740. https://doi.org/10.1021/acsami.7b06253
31. Balamurugan C, Arunkumar S, Lee DW (2016) Hierarchical 3D nanostructure of $GdInO_3$ and reduced-graphene-decorated $GdInO_3$ nanocomposite for CO sensing applications. Sens Actuators B Chem 234:155–166. https://doi.org/10.1016/j.snb.2016.04.043
32. Shanmugasundaram A, Kim DS, Chinh ND, Park J, Jeong YJ, Piao J, Kim D, Lee DW (2021) N-/S-dual doped C@ ZnO: an excellent material for highly selective and responsive NO_2 sensing at ambient temperatures. Chem Eng J 421:127740. https://doi.org/10.1016/j.cej.2020.127740
33. Li C, Choi PG, Masuda Y (2023) Large-lateral-area SnO2 nanosheets with a loose structure for high-performance acetone sensor at the ppt level. J Hazard Mater 455:131592. https://doi.org/10.1016/j.jhazmat.2023.131592
34. Wang W, Xian J, Li J, Yu M, Duan Q, Leung CM, Zeng M, Gao X (2024) Construction of Co3O4/SnO2 yolk-shell nanofibers for acetone gas detection. Sens Actuators B Chem 398:134724. https://doi.org/10.1016/j.snb.2023.134724
35. Li C, Kim K, Fuchigami T, Asaka T, Kakimoto KI, Masuda Y (2023) Acetone gas sensor based on Nb2O5@ SnO2 hybrid structure with high selectivity and ppt-level sensitivity. Sens Actuators B Chem. https://doi.org/10.1016/j.snb.2023.134144
36. Song BY, Huang J, Cui ZQ, Zhang XF, Deng ZP, Xu YM, Gao HLH, S, (2023) Temperature-controlled dual-selectivity nitric oxide/acetone sensor constructed from mesoporous SnO2 tubes doped by biomass-derived graphitic carbon. Appl Surf Sci 623:157009. https://doi.org/10.1016/j.apsusc.2023.157009
37. Zhang H, Guo S, Zheng W, Wang H, Li HY, Yu MH, Chang Z, Liu BuXH, H, (2023) Facile engineering of metal–organic framework derived SnO2-ZnO composite based gas sensor toward superior acetone sensing performance. J Chem Eng. https://doi.org/10.1016/j.cej.2023.143927
38. Bulemo PM, Kim DH, Kim ID (2021) Controlled synthesis of electrospun hollow Pt-loaded SnO2 microbelts for acetone sensing. Sens Actuators B Chem 344:130208. https://doi.org/10.1016/j.snb.2021.130208
39. Guo L, Shen Z, Ma C, Ma C, Wang J, Yuan T (2022) Gas sensor based on MOFs-derived Au-loaded SnO2 nanosheets for enhanced acetone detection. J Alloys Compd 906:164375. https://doi.org/10.1016/j.jallcom.2022.164375
40. Jin S, Wu D, Song W, Hao H, Gao W, Yan S (2022) Superior acetone sensor based on hetero-interface of SnSe2/SnO2 quasi core shell nanoparticles for previewing diabetes. J Colloid Interface Sci 621:119–130. https://doi.org/10.1016/j.jcis.2022.04.057
41. He L, Hu J, Yuan Q, Xia Z, Jin L, Gao H, Fan L, Chu X, Meng F (2023) Synthesis of porous ZnFe2O4/SnO2 core-shell spheres for high-performance acetone gas sensing. Sens Actuators B Chem 378:133123. https://doi.org/10.1016/j.snb.2022.133123
42. Xu S, Wang M, Chen CP, Feng S (2023) Sea urchin-like SnO_2/α-Fe_2O_3 hetero structural microspheres for enhanced acetone gas sensing: materials preparation, performance evaluation, and mechanism investigation. Sens Actuators B Chem 379:133288. https://doi.org/10.1016/j.snb.2023.133288
43. Hao S, Wang H, Yang R, Liu D, Wan J, Liu X, Zhang Q, Chen X (2021) Dandelion-like SiO_2@ SnO_2/α-Fe_2O_3 hollow spheres formed by growing of α-Fe_2O_3 nanotubes on low crystalline SiO_2@ SnO_2 and their enhanced acetone-sensing properties. Sens Actuators B Chem 329:129152. https://doi.org/10.1016/j.snb.2020.129152
44. Lu J, Xie Y, Luo F, Fu H, Huang X, Liu Y, Liu H (2020) Heterostructures of mesoporous hollow Zn_2SnO_4/SnO_2 microboxes for high-performance acetone sensors. J Alloys Compd 844:155788. https://doi.org/10.1016/j.jallcom.2020.155788
45. Hu J, Yang J, Wang W, Xue Y, Sun Y, Li P, Lian K, Zhang W, Chen L, Shi J, Chen Y (2018) Synthesis and gas sensing properties of NiO/SnO_2 hierarchical structures toward ppb-level acetone detection. Mater Res Bull 102:294–303. https://doi.org/10.1016/j.materresbull.2018.02.006
46. Xu X, Chen Y, Zhang G, Ma S, Lu Y, Bian H, Chen Q (2017) Highly sensitive VOCs-acetone sensor based on Ag-decorated SnO_2 hollow nanofibers. J Alloys Compd 703:572–579. https://doi.org/10.1016/j.jallcom.2017.01.348
47. Wang T, Cheng L (2021) Hollow hierarchical TiO_2-SnO_2-TiO_2 composite nanofibers with increased active-sites and charge transfer for enhanced acetone sensing performance. Sens Actuators B Chem 334:129644. https://doi.org/10.1016/j.snb.2021.129644
48. Jiang Z, Wang C, Yang Z, Zhang L, Jin J, Guo X, Zhong L, Duan Z, Li H (2021) Electrospun Eu_2O_3/Au/SnO_2 ternary nanofibers with synergistically enhanced acetone sensing properties. Mater Lett 304:130729. https://doi.org/10.1016/j.matlet.2021.130729
49. Liu M, Song P, Yang Z, Wang Q (2021) Hierarchical assembly of SnO_2 nanorod on spindle-like α-Fe_2O_3 for enhanced acetone gas-sensing performance. Ceram Int 47(9):12181–12188. https://doi.org/10.1016/j.ceramint.2021.01.065
50. Jiang Z, Zhao R, Sun B, Nie G, Ji H, Lei J, Wang C (2016) Highly sensitive acetone sensor based on Eu-doped SnO_2 electrospun nanofibers. Ceram Int 42(14):15881–15888. https://doi.org/10.1016/j.ceramint.2016.07.060
51. Cheng L, Ma SY, Wang TT, Luo J (2015) Synthesis and enhanced acetone sensing properties of 3D porous flower-like SnO_2 nanostructures. Mater, Lett 143:84–87. https://doi.org/10.1016/j.matlet.2014.12.062
52. Tomer VK, Singh K, Kaur H, Shorie M, Sabherwal P (2017) Rapid acetone detection using indium loaded WO3/SnO2 nanohybrid sensor. Sens Actuators B Chem 253:703–713. https://doi.org/10.1016/j.snb.2017.06.179
53. Wang Q, Yao N, An D, Li Y, Zou Y, Lian X, Tong X (2016) Enhanced gas sensing properties of hierarchical SnO_2 nanoflower assembled from nanorods via a one-pot template-free hydrothermal method. Ceram Int 42(14):15889–15896. https://doi.org/10.1016/j.ceramint.2016.07.062
54. Cheng L, Ma SY, Wang TT, Luo J (2015) Synthesis and enhanced acetone sensing properties of 3D porous flower-like SnO_2 nanostructures. Mater Lett 143:84–87. https://doi.org/10.1016/j.matlet.2014.12.062
55. Wang TT, Ma SY, Cheng L, Jiang XH, Zhang M, Li WQ, Jin WX (2016) Facile fabrication of multishelled SnO_2 hollow microspheres for gas sensing application. Mater Lett 164:56–59. https://doi.org/10.1016/j.matlet.2015.10.118
56. Li WQ, Ma SY, Luo J, Mao YZ, Cheng L, Gengzang DJ, Xu XL, Yan SH (2014) Synthesis of hollow SnO_2 nanobelts and their application in acetone sensor. Mater Lett 132:338–341. https://doi.org/10.1016/j.matlet.2014.06.112
57. Li X, Liu Y, Li S, Huang J, Wu Y, Yu D (2016) The sensing properties of single Y-doped SnO_2 nanobelt device to acetone. Nanoscale Res Lett 11:1–8
58. Yu H, Wang S, Xiao C, Xiao B, Wang P, Li Z, Zhang M (2015) Enhanced acetone gas sensing properties by aurelia-like SnO_2 micro-nanostructures. CrystEngComm 17(23):4316–4324. https://doi.org/10.1039/C5CE00448A
59. Shanmugasundaram A, Manorama SV, Kim DS, Jeong YJ, Lee DW (2022) Toward point-of-Care chronic disease management: biomarker detection in exhaled breath using an E-Nose sensor based on rGO/ SnO_2 superstructures. J Chem Eng 448:137736. https://doi.org/10.1016/j.cej.2022.137736
60. Boppella R, Manjula P, Arunkumar S, Manorama SV (2014) Advances in synthesis of nanostructured metal oxides for chemical sensors. Chem Sens 4:19
61. Arunkumar S, Basak P, Satyanarayana L, Manorama SV (2012) 4.3. 5 One-pot hydrothermal synthesis of SnO and SnO2 nanostructures: enhanced H2 sensing attributed to in-situ pn junctions. Proc IMCS 22:372–375
62. Shanmugasundaram A, Lee DW (2022) SnO_2/rGO nanocomposite for the detection of biomarkers of lung cancer. Micro Nano Syst Lett 10(1):1–9. https://doi.org/10.1186/s40486-022-00154-7
63. Abdelghani R, Hassan HS, Morsi I, Kashyout AB (2019) Nano-architecture of highly sensitive SnO_2–based gas sensors for acetone and ammonia using molecular imprinting technique. Sens Actuators B Chem 297:126668. https://doi.org/10.1016/j.snb.2019.126668
64. Zhang X, Xu G, Wang H, Cui H, Zhan X, Wang X (2019) Enhanced acetone sensing properties of hollow SnO_2 fibers using poplar catkins as a bio-template. Powder Techno 344:183–189. https://doi.org/10.1016/j.powtec.2018.12.020
65. Cheng P, Wang C, Wang Y, Xu L, Dang F, Lv L, Li X (2021) Enhanced acetone sensing properties based on in situ growth SnO_2 nanotube arrays. Nanotechnology 32(24):245503. https://doi.org/10.1088/1361-6528/abed74/meta

66. Kim K, Choi PG, Itoh T, Masuda Y (2020) Catalyst-free highly sensitive SnO_2 nanosheet gas sensors for parts per billion-level detection of acetone. ACS Appl Mater Interfaces 12(46):51637. https://doi.org/10.1021/acsami.0c15273
67. Li Y, Qiao L, Yan D, Wang L, Zeng Y, Yang H (2014) Preparation of Au-sensitized 3D hollow SnO_2 microspheres with an enhanced sensing performance. J Alloys Compd 586:399–403. https://doi.org/10.1016/j.jallcom.2013.09.147
68. Cheng JP, Wang BB, Zhao MG, Liu F, Zhang XB (2014) Nickel-doped tin oxide hollow nanofibers prepared by electrospinning for acetone sensing. Sens Actuators B Chem 190:78–85. https://doi.org/10.1016/j.snb.2013.08.098
69. Kou X, Xie N, Chen F, Wang T, Guo L, Wang C, Wang Q, Ma J, Sun Y, Zhang H, Lu G (2018) Superior acetone gas sensor based on electrospun SnO_2 nanofibers by Rh doping. Sens Actuators B Chem 256:861–869. https://doi.org/10.1016/j.snb.2017.10.011
70. Ahmadnia-Feyzabad S, Khodadadi AA, Vesali-Naseh M, Mortazavi Y (2012) Highly sensitive and selective sensors to volatile organic compounds using MWCNTs/SnO_2. Sens Actuators B Chem 166:150–155. https://doi.org/10.1016/j.snb.2012.02.024
71. Choi SJ, Jang BH, Lee SJ, Min BK, Rothschild A, Kim ID (2014) Selective detection of acetone and hydrogen sulfide for the diagnosis of diabetes and halitosis using SnO_2 nanofibers functionalized with reduced graphene oxide nanosheets. ACS Appl Mater Inter 6(4):2588–2597. https://doi.org/10.1021/am405088q
72. Singkammo S, Wisitsoraat A, Sriprachuabwong C, Tuantranont A, Phanichphant S, Liewhiran C (2015) Electrolytically exfoliated graphene-loaded flame-made Ni-doped SnO_2 composite film for acetone sensing. ACS Appl Mater Inter 7(5):3077–3092. https://doi.org/10.1021/acsami.5b00161
73. Xu Y, Zheng L, Yang C, Liu X, Zhang J (2020) Highly sensitive and selective electronic sensor based on Co catalyzed SnO_2 nanospheres for acetone detection. Sens Actuators B Chem 304:127237. https://doi.org/10.1016/j.snb.2019.127237
74. Jiang Z, Yin M, Wang C (2017) Facile synthesis of Ca^{2+}/Au co-doped SnO_2 nanofibers and their application in acetone sensor. Mater Lett 194:209–212. https://doi.org/10.1016/j.matlet.2017.02.031
75. Lian X, Li Y, Tong X, Zou Y, Liu X, An D, Wang Q (2017) Synthesis of Ce-doped SnO_2 nanoparticles and their acetone gas sensing properties. Appl Surf Sci 407:447–455. https://doi.org/10.1016/j.apsusc.2017.02.228
76. Cheng L, Ma SY, Li XB, Luo J, Li WQ, Li FM, Mao YZ, Wang TT, Li YF (2014) Highly sensitive acetone sensors based on Y-doped SnO_2 prismatic hollow nanofibers synthesized by electrospinning. Sens Actuators B Chem 200:181–190. https://doi.org/10.1016/j.snb.2014.04.063
77. Hu J, Xiong X, Guan W, Tan C (2022) Hollow mesoporous SnO_2/Zn_2SnO_4 heterojunction and RGO decoration for high-performance detection of acetone. ACS Appl Mater Inter 14(49):55249–55263. https://doi.org/10.1021/acsami.2c18255
78. Wang Z, Wang F, Hermawan A, Asakura Y, Hasegawa T, Kumagai H, Kato H, Kakihana M, Zhu J, Yin S (2021) SnO- SnO_2 modified two-dimensional MXene Ti_3C_2Tx for acetone gas sensor working at room temperature. J Mater Sci Technol 73:128–138. https://doi.org/10.1016/j.jmst.2020.07.040
79. Kwak CH, Kim TH, Jeong SY, Yoon JW, Kim JS, Lee JH (2018) Humidity-independent oxide semiconductor chemiresistors using terbium-doped SnO_2 yolk–shell spheres for real-time breath analysis. ACS Appl Mater Inter 10(22):18886–18894. https://doi.org/10.1021/acsami.8b04245
80. Cho HJ, Choi SJ, Kim NH, Kim ID (2020) Porosity controlled 3D SnO_2 spheres via electrostatic spray: selective acetone sensors. Sen Actuators B Chem 304:127350. https://doi.org/10.1016/j.snb.2019.127350
81. Jang JS, Choi SJ, Kim SJ, Hakim M, Kim ID (2016) Rational design of highly porous SnO_2 nanotubes functionalized with biomimetic nanocatalysts for direct observation of simulated diabetes. Adv Funct Mater 26(26):4740–4748. https://doi.org/10.1002/adfm.201600797
82. Li G, Cheng Z, Xiang Q, Yan L, Wang X, Xu J (2019) Bimetal PdAu decorated SnO_2 nanosheets based gas sensor with temperature-dependent dual selectivity for detecting formaldehyde and acetone. Sen Actuators B Chem 283:590–601. https://doi.org/10.1016/j.snb.2018.09.117
83. Li J, Xian J, Wang W, Cheng K, Zeng M, Zhang A, Wu S, Gao X, Lu X, Liu JM (2022) Ultrafast response and high-sensitivity acetone gas sensor based on porous hollow Ru-doped SnO_2 nanotubes. Sen Actuators B Chem 352:131061. https://doi.org/10.1016/j.snb.2021.131061
84. Kou X, Meng F, Chen K, Wang T, Sun P, Liu F, Yan X, Sun Y, Liu F, Shimanoe K, Lu G (2020) High-performance acetone gas sensor based on Ru-doped SnO_2 nanofibers. Sen Actuators B Chem 320:128292. https://doi.org/10.1016/j.snb.2020.128292
85. Lian D, Shi B, Dai R, Jia X, Wu X (2017) Synthesis and enhanced acetone gas-sensing performance of $ZnSnO_3$/ SnO_2 hollow urchin nanostructures. J Nanopart Res 19:1–8
86. Cheng P, Lv L, Wang Y, Zhang B, Zhang Y, Zhang Y, Lei Z, Xu L (2021) SnO_2/$ZnSnO_3$ double-shelled hollow microspheres based high-performance acetone gas sensor. Sen Actuators B Chem 332:129212. https://doi.org/10.1016/j.snb.2020.129212
87. Punginsang M, Wisitsora-At A, Tuantranont A, Phanichphant S, Liewhiran C (2015) Effects of cobalt doping on nitric oxide, acetone and ethanol sensing performances of FSP-made SnO_2 nanoparticles. Sen Actuators B Chem 210:589–601. https://doi.org/10.1016/j.snb.2015.01.028
88. Yan SH, Ma SY, Xu XL, Li WQ, Luo J, Jin WX, Wang TT, Jiang XH, Lu Y, Song HS (2015) Preparation of SnO_2–ZnO hetero-nanofibers and their application in acetone sensing performance. Mater Lett 159:447–450. https://doi.org/10.1016/j.matlet.2015.07.051
89. Li F, Zhang T, Gao X, Wang R, Li B (2017) Coaxial electrospinning heterojunction SnO_2/Au-doped In_2O_3 core-shell nanofibers for acetone gas sensor. Sen Actuators B Chem 252:822–830. https://doi.org/10.1016/j.snb.2017.06.077
90. Zhang D, Liu A, Chang H, Xia B (2015) Room-temperature high-performance acetone gas sensor based on hydrothermal synthesized SnO_2-reduced graphene oxide hybrid composite. Rsc Adv 5(4):3016–3022. https://doi.org/10.1039/C4RA10942B
91. Chen L, Song Y, Liu W, Dong H, Wang D, Liu J, Liu Q, Chen X (2022) MOF-based nanoscale Pt catalyst decorated SnO_2 porous nanofibers for acetone gas detection. J Alloys Compd 893:162322. https://doi.org/10.1016/j.jallcom.2021.162322
92. Li F, Gao X, Wang R, Zhang T, Lu G (2017) Study on TiO_2- SnO_2 core-shell heterostructure nanofibers with different work function and its application in gas sensor. Sen Actuators B Chem 248:812–819. https://doi.org/10.1016/j.snb.2016.12.009
93. Koo WT, Jang JS, Choi SJ, Cho HJ, Kim ID (2017) Metal–organic framework templated catalysts: dual sensitization of PdO–ZnO composite on hollow SnO_2 nanotubes for selective acetone sensors. ACS Appl Mater Inter 9(21):18069–18077. https://doi.org/10.1021/acsami.7b04657
94. Shin J, Choi SJ, Lee I, Youn DY, Park CO, Lee JH, Tuller HL, Kim ID (2013) Thin-wall assembled SnO_2 fibers functionalized by catalytic Pt nanoparticles and their superior exhaled-breath-sensing properties for the diagnosis of diabetes. Adv Funct Mater 23(19):2357–2367. https://doi.org/10.1002/adfm.201202729
95. Jang JS, Kim SJ, Choi SJ, Kim NH, Hakim M, Rothschild A, Kim ID (2015) Thin-walled SnO_2 nanotubes functionalized with Pt and Au catalysts via the protein templating route and their selective detection of acetone and hydrogen sulfide molecules. Nanoscale 7(39):16417–16426. https://doi.org/10.1039/C5NR04487A
96. Wang P, Wang S-Z, Han Q, Zou D-Q, Zhao W-K, Wang X-D, Luo C, Yang X, Wu X, Xie W-F (2021) Construction of hierarchical α-Fe2O3/SnO2 nanoball arrays with superior acetone sensing performance. Adv Mater Interfaces 8:2001831
97. Kim DH, Jang JS, Koo WT, Choi SJ, Kim SJ, Kim ID (2018) Hierarchically interconnected porosity control of catalyst-loaded WO_3 nanofiber scaffold: Superior acetone sensing layers for exhaled breath analysis. Sen Actuators B Chem 259:616–625. https://doi.org/10.1016/j.snb.2017.12.051
98. Wang D, Huang S, Li H, Chen A, Wang P, Yang J, Wang X, Yang J (2019) Ultrathin WO_3 nanosheets modified by g-C_3N_4 for highly efficient acetone vapor detection. Sen Actuators B Chem 282:961–971. https://doi.org/10.1016/j.snb.2018.11.138
99. Li Y, Hua Z, Wu Y, Zeng Y, Qiu Z, Tian X, Wang M, Li E (2018) Modified impregnation synthesis of Ru-loaded WO_3 nanoparticles for acetone sensing. Sen Actuators B Chem 265:249–256. https://doi.org/10.1016/j.snb.2018.03.037
100. Chen L, Huang L, Lin Y, Sai L, Chang Q, Shi W, Chen Q (2018) Fully gravure-printed WO_3/Pt-decorated rGO nanosheets composite film for

detection of acetone. Sen Actuators B Chem 255:1482–1490. https://doi.org/10.1016/j.snb.2017.08.158
101. Shen JY, Wang MD, Wang YF, Hu JY, Zhu Y, Zhang YX, Li ZJ, Yao HC (2018) Iron and carbon codoped WO_3 with hierarchical walnut-like microstructure for highly sensitive and selective acetone sensor. Sen Actuators B Chem 256:27–37. https://doi.org/10.1016/j.snb.2017.10.073
102. Righettoni M, Tricoli A, Pratsinis SE (2010) Si: WO_3 sensors for highly selective detection of acetone for easy diagnosis of diabetes by breath analysis. Anal Chem 82(9):3581–3587. https://doi.org/10.1021/ac902695n
103. Wang P, Wang D, Zhang M, Zhu Y, Xu Y, Ma X, Wang X (2016) ZnO nanosheets/graphene oxide nanocomposites for highly effective acetone vapor detection. Sen Actuators B Chem 230:477–484. https://doi.org/10.1016/j.snb.2016.02.056
104. Jia Q, Ji H, Zhang Y, Chen Y, Sun X, Jin Z (2014) Rapid and selective detection of acetone using hierarchical ZnO gas sensor for hazardous odor markers application. J Hazard Mater 276:262–270. https://doi.org/10.1016/j.jhazmat.2014.05.044
105. Liu W, Xie Y, Chen T, Lu Q, Rehman SU, Zhu L (2019) Rationally designed mesoporous In_2O_3 nanofibers functionalized Pt catalysts for high-performance acetone gas sensors. Sen Actuators B Chem 298:126871. https://doi.org/10.1016/j.snb.2019.126871
106. Navale ST, Yang ZB, Liu C, Cao PJ, Patil VB, Ramgir NS, Mane RS, Stadler FJ (2018) Enhanced acetone sensing properties of titanium dioxide nanoparticles with a sub-ppm detection limit. Sen Actuators B Chem 255:1701–1710. https://doi.org/10.1016/j.snb.2017.08.186
107. Zhou T, Zhang T, Deng J, Zhang R, Lou Z, Wang L (2017) P-type Co_3O_4 nanomaterials-based gas sensor: preparation and acetone sensing performance. Sen Actuators B Chem 242:369–377. https://doi.org/10.1016/j.snb.2016.11.067
108. Yang M, Lu J, Wang X, Zhang H, Chen F, Sun J, Yang J, Sun Y, Lu G (2020) Acetone sensors with high stability to humidity changes based on Ru-doped NiO flower-like microspheres. Sen Actuators B Chem 313:127965. https://doi.org/10.1016/j.snb.2020.127965
109. Mirzaei A, Janghorban K, Hashemi B, Bonyani M, Leonardi SG, Neri G (2016) A novel gas sensor based on Ag/Fe_2O_3 core-shell nanocomposites. Ceram Int 42(16):18974–18982. https://doi.org/10.1016/j.ceramint.2016.09.052

Publisher's Note

Springer Nature remains neutral with regard to jurisdictional claims in published maps and institutional affiliations.

Submit your manuscript to a SpringerOpen journal and benefit from:

- ► Convenient online submission
- ► Rigorous peer review
- ► Open access: articles freely available online
- ► High visibility within the field
- ► Retaining the copyright to your article

Submit your next manuscript at ► springeropen.com